
Electronic Thesis and Dissertation Repository

8-11-2022 1:00 PM

Identification and characterization of novel fumonisin-detoxifying enzymes

Michael C. Kovacevic, *The University of Western Ontario*

Supervisor: Garnham, Christopher, *Agriculture and Agri-Food Canada*

Co-Supervisor: Junop, Murray, *The University of Western Ontario*

A thesis submitted in partial fulfillment of the requirements for the Master of Science degree in Biochemistry

© Michael C. Kovacevic 2022

Follow this and additional works at: <https://ir.lib.uwo.ca/etd>



Part of the [Biochemistry, Biophysics, and Structural Biology Commons](#)

Recommended Citation

Kovacevic, Michael C., "Identification and characterization of novel fumonisin-detoxifying enzymes" (2022). *Electronic Thesis and Dissertation Repository*. 8739.

<https://ir.lib.uwo.ca/etd/8739>

This Dissertation/Thesis is brought to you for free and open access by Scholarship@Western. It has been accepted for inclusion in Electronic Thesis and Dissertation Repository by an authorized administrator of Scholarship@Western. For more information, please contact wlsadmin@uwo.ca.

Abstract

Fumonisinins are a family of mycotoxins produced by *Aspergillus* and *Fusarium* spp. fungi whose contamination of food and feed presents a worldwide agro-economic threat. Certain *Aspergillus* spp. post-biosynthetically convert their B series fumonisinins (FB) to less toxic forms, replacing their terminal amine with a ketone (FPy) or hydroxyl (FLa). AnFAO is an enzyme responsible for FB deamination in *Aspergilli*, however FLa-generating enzymes remain unknown. Additionally, *Fusarium*'s potential fumonisin-detoxifying ability has not been characterized. Herein, I identify FLa-generating enzymes (FUM13) and characterize the fumonisin-deaminating activity of an *F. verticillioides* AnFAO homolog (FvFAO). *A. niger* and *F. verticillioides* FUM13 isoforms reduced FPy fumonisinins to FLa forms overnight with low efficiency. I also report that FvFAO deaminates FB fumonisinins ~5x less efficiently than AnFAO. These results provide insight into differences in fumonisin self-protection mechanisms between these genera, and may lead to the development of new tools for treatment of fumonisin-contaminated food and feed.

Keywords

Mycotoxin, fumonisin, *Aspergillus niger*, *Aspergillus welwitschiae*, *Fusarium verticillioides*, detoxification, deamination, oxidoreduction, chromatography, mass spectrometry, agriculture, biotransformation, kinetics, fungi.

Summary for Lay Audience

Mycotoxins are toxic secondary metabolites produced by crop-dwelling fungi. They are not required for growth and development, however, they help fungi break down plant matter to more easily absorb nutrients. Fumonisin is a family of mycotoxins produced by various *Fusarium* and *Aspergillus* species. Their colonization of various crops, and subsequent fumonisin production, presents a significant agro-economic threat as they are associated with many diseases in plants, animals, and humans.

B series fumonisins (FB) are the most abundant and most toxic. They are composed of a linear poly-carbon backbone with many functional groups, one of the most important being a terminal amine ($-NH_2$). This amine is primarily responsible for their toxicity, allowing FB fumonisins to inhibit ceramide synthase, an enzyme involved in sphingolipid biosynthesis.

Notably, certain *Aspergillus* spp. convert their FB fumonisins to less toxic FPy and FLA forms. Their only difference is the replacement of the amine by a carbonyl ($=O$) in the FPy form, and a hydroxyl ($-OH$) in the FLA form. Our lab hypothesized that there is a sequential, enzymatic detoxification process where FB fumonisins are converted to FPy forms, which are then converted to FLA forms. The enzyme responsible for FB to FPy conversion has already been identified and characterized. However, the FLA-generating enzyme(s) remained unknown.

In this thesis, I identify an enzyme from *A. niger* and *F. verticillioides* (FUM13) capable of FPy to FLA conversion. FUM13 converts the FPy carbonyl to the FLA hydroxyl *in vitro*, albeit very slowly. Importantly, this work led to the investigation of *F. verticillioides*' potential to post-biosynthetically modify its own fumonisins.

Neither FPy nor FLA production by *F. verticillioides* has previously been reported in the literature. However in this thesis, in addition to identifying an *F. verticillioides* FLA-generating enzyme for the first time, I biochemically characterize the newly discovered FPy-generating activity of an additional *F. verticillioides* enzyme (FvFAO). Overall, this work adds to our growing understanding of fumonisin self-protection methods in *Fusaria* and *Aspergilli*, and provides a starting point for the development of new tools to mitigate fumonisin contamination in food and feed.

List of Abbreviations

AAFC: Agriculture and Agri-Food Canada
AGC: Automatic gain control
AMS: Ammonium sulfate
A. niger: *Aspergillus niger*
AnFAO: *Aspergillus niger* Fumonisin Amine Oxidase
A. welwitschiae: *Aspergillus welwitschiae*
BGC: Biosynthetic gene cluster
BLAST: Basic Local Alignment Search Tool
CER: Ceramide synthase gene (e.g. CER1)
CoA: Coenzyme A
CV: Column volume
DDA: Data dependent acquisition
DDGS: Dried distillers' grains and solubles
DMSO: Dimethyl sulfoxide
DON: Deoxynivalenol
DTT: Dichlorodiphenyltrichloroethane
EU: European Union
FAD: Flavin adenine dinucleotide
FAO: Food and Agriculture Organization of the United Nations
F. verticillioides: *Fusarium verticillioides*
FB: Fumonisin B series (e.g. FB₁)
FPy: Fumonisin Py series (e.g. FPy₁)
FLa: Fumonisin La series (e.g. FLa₁)
FUM: Fumonisin biosynthetic gene (e.g. FUM1)
FvFAO: *Fusarium verticillioides* Fumonisin Amine Oxidase
GST: Glutathione S-transferase
HESI: Heated electrospray ionization
HPLC: High-performance liquid chromatography
HRP: Horseradish peroxidase
IARC: International Agency of Research on Cancer

IPTG: Isopropyl β -D-1-thiogalactopyranoside
IT: Injection time
LC-MS: Liquid chromatography-mass spectrometry
LIC: Ligation independent cloning
MAO: Monoamine oxidase
MBP: Maltose-binding protein
MEA: Malt extract agar
MEGAWHOP: Megaprimer PCR of Whole Plasmid
MES: N-morpholino ethanesulfonic acid
MW: Molecular weight
NADH: Nicotinamide adenine dinucleotide
NADPH: Nicotinamide adenine dinucleotide phosphate
Ni-IMAC: Nickel immobilized metal affinity chromatography
OD: Optical density
OTA: Ochratoxin A
OT α : Ochratoxin α
PBS: Phosphate-buffered saline
PCR: Polymerase Chain Reaction
PDB: Protein Data Bank
SDR: Short-chain dehydrogenase/reductase
SDS-PAGE: Sodium dodecyl-sulfate polyacrylamide gel electrophoresis
SEC: Size-exclusion chromatography
TB: Terrific broth
TCE: Tricarballic ester
TEV: Tobacco etch virus
WT: Wild type
YES: Yeast extract sucrose
YPD: Yeast extract peptone dextrose
YPDS: Yeast extract peptone dextrose sucrose

Acknowledgments

I would first like to thank my family for their ever-present support during my academic journey thus far; both my mom & dad, my brothers Christian & Thomas, and my present and late grandparents, Baka & Dida and Oma & Opa. I would also like to thank my friends for their encouragement and comic relief over the past two years, especially Tyson for his constant checking-in to see if I had “found the corn bandit yet”.

One of my biggest thank you’s must go to Dr. Pat Telmer, not only for his help over the duration of my MSc, but also for his camaraderie in the lab, especially during the COVID pandemic. Your guidance, whether for large experiments, or simpler, every-day questions, is a huge reason I am here today. Thank you as well to past and present members of the Garnham and Sumarah labs for their assistance and friendship, especially Angelo, Shane, Jacob, Cam, Natasha, and Shawn. I could not forget to thank Dr. Justin Renaud for all his mass spectrometry-related help, especially for developing fumonisin analysis methods, and Megan Kelman for all her help with the mass spectrometer and for her training & advice regarding fungal cultures.

As well, a huge thank you to my amazing mentor and supervisor, Dr. Christopher Garnham. Your guidance and willingness to teach over the past two years has been invaluable. Thank you for pushing me to fulfill my potential as a scientist, and for allowing me the freedom to contribute to the structure of my project.

I would also like to thank my co-supervisor, Dr. Murray Junop, not only for your support during my MSc, but for your constant positivity and encouragement ever since my fourth-year undergraduate project in your lab. Thank you as well to all members

of the Junop lab, especially Ryan Grainger, for your assistance and for accommodating me at the beginning of my MSc when COVID restrictions did not allow me to work at the AAFC research centre.

Finally, thank you to the other members of my advisory committee, Dr. Mark Sumarah and Dr. Caroline Schild-Poulter for your guidance, insight, and suggestions over the past two years.

Table of Contents

Abstract	ii
Keywords	iii
Summary for Lay Audience.....	iv
List of Abbreviations	vi
Acknowledgments.....	viii
Table of Contents.....	x
List of Tables	xii
List of Figures	xiii
Chapter 1 – Introduction	1
1.1 Mycotoxins.....	1
1.2 Fumonisin	3
1.2.1 <i>Fusarium</i> and <i>Aspergillus</i> spp. Fumonisin Production.....	3
1.2.2 Fumonisin Structure and Toxicity	4
1.3 Mycotoxin Prevention and Detoxification Strategies	7
1.4 Fumonisin Toxicity Defense in <i>Fusaria</i> vs. <i>Aspergilli</i>	8
1.4.1 Fumonisin Poisoning Resistance in <i>Fusaria</i>	9
1.4.2 Post-Biosynthetic Fumonisin Detoxification in <i>Aspergilli</i>	10
1.5 Experimental Approach and Objectives.....	11
Chapter 2 – Materials and Methods	13
2.1 LC-MS Screening of Fungal Culture Supernatants	13
2.2 FPy Synthesis	15
2.3 Reverse-Phase Fumonisin Extraction	15
2.4 Fungal Protoplast Preparation & Assays	16
2.5 Expression Vectors.....	17

2.5.1 Construct Design and Engineering	17
2.5.2 Cloning and Vectors	17
2.5.3 Site-Directed Mutagenesis	18
2.6 Protein Expression and Purification.....	18
2.6.1 Protein Expression	18
2.6.2 Protein Purification	19
2.7 LC-MS Detection of Enzymatically Modified Fumonisin.....	19
2.8 Amplex™ Red Relative Rate and Kinetic Assays.....	20
Chapter 3 – Results	22
3.1 Fungal Culture Fumonisin Screening.....	22
3.2 FLa Production by <i>A. welwitschiae</i> Protoplasts.....	29
3.3 Analysis of FLa-Generating Enzyme Candidates	31
3.3.1 <i>A. niger</i> sdr1	32
3.3.2 <i>A. niger</i> FUM13	41
3.3.3 <i>F. verticillioides</i> FUM13	46
3.4 Discovery of an FPy-Generating <i>F. verticillioides</i> Amine Oxidase	53
3.5 Biochemical Characterization of <i>F. verticillioides</i> Amine Oxidase FvFAO	56
3.5.1 Relative Rates for FvFAO vs. AnFAO	57
3.5.2 Kinetic Analyses of FvFAO.....	59
Chapter 4 – Discussion	62
4.1 Characteristics of FLa-Generating Enzymes	62
4.2 Fumonisin Detoxification in <i>Aspergilli</i> vs. <i>Fusaria</i> : Newly Discovered Enzymes & Functions lead to New Questions.....	67
4.3 Conclusions and Future Directions	73
References.....	78
Curriculum Vitae	83

List of Tables

Table 1	59
Table 2	61

List of Figures

Figure 1	3
Figure 2	4
Figure 3	6
Figure 4	11
Figure 5	23
Figure 6	26
Figure 7	27
Figure 8	31
Figure 9	33
Figure 10	34
Figure 11	34
Figure 12	35
Figure 13	37
Figure 14	38
Figure 15	39
Figure 16	40
Figure 17	42
Figure 18	43
Figure 19	44
Figure 20	45
Figure 21	47
Figure 22	49
Figure 23	50
Figure 24	51
Figure 25	52
Figure 26	53
Figure 27	54
Figure 28	55
Figure 29	58
Figure 30	60

Chapter 1 – Introduction

1.1 Mycotoxins

Mycotoxins are small-molecule secondary metabolites produced by filamentous fungi that are toxic to humans and animals, and can be lethal when consumed at high concentrations^{1,2}. These compounds are not required for growth or development, but their production by crop-dwelling fungi presents a significant agricultural, economic, and potential public health threat.

The *Aspergillus*, *Fusarium*, *Penicillium*, and *Alternaria* genera are primarily responsible for mycotoxin production, and therefore pose the greatest agro-economic threat³. Mycotoxin production by these fungi renders them phytotoxic and provides a selective advantage; allowing them to harm competing organisms as well as their plant hosts. These pathogenic fungi colonize a variety of hosts, however crops such as corn and wheat, as well as grapes, are the most common⁴. A previous estimate from the Food and Agriculture Organization of the United Nations (FAO) suggests that over 25% of global food crops are contaminated with mycotoxins⁵. That is, roughly one quarter of the world's crops are estimated to contain mycotoxin levels exceeding the regulatory standards of the European Union (EU) and Codex Alimentarius Commission. With recent advances in analytical chemistry technology, as well as the impact of climate change, this estimate grows to 60-80% for crops that contain mycotoxins above detectable levels, illustrating the threat they pose without stringent control measures.

The most common and widely studied mycotoxins fall into one of five families: aflatoxins, trichothecenes, zearalenone, ochratoxins, and fumonisins. Each

family has a characteristic chemical backbone that serves as a scaffold for functional groups that differentiate individual congeners based on position and type (Figure 1)⁴. Their unique structures determine the biological targets each family can inhibit, dictating their toxic properties.

Aflatoxin B₁, one of the most dangerous mycotoxins to humans, produced mainly by *Aspergillus flavus* and *A. parasiticus*, is carcinogenic, teratogenic, and immunosuppressive^{4,6}. In comparison, deoxynivalenol (DON), the most common trichothecene produced by a limited number of *Fusarium* species, inhibits protein synthesis and therefore poses a threat to actively dividing cells⁷. Due to its relatively high prevalence in small grain cereals and its nephrotoxic effects in humans, DON is the mycotoxin of greatest concern in North America^{4,8}. To illustrate, data from the 2019 BIOMIN world mycotoxin survey showed that DON was detected in 79% of crop and soil samples tested from this continent. In contrast, the risk of zearalenone toxicity in humans is generally low, however this mycotoxin is often co-produced by the same organisms as DON and has been shown to have estrogenic-like effects in farm animals, especially pigs⁹. Ochratoxin A (OTA) is the most common and most toxic congener of the ochratoxin family, produced mainly by grape-colonizing *Aspergilli* such as *A. carbonarius* and *A. ochraceus*. It is primarily nephrotoxic, but also thought to be hepatotoxic at high concentrations. For example, Balkan Endemic Nephropathy, a human kidney disease also associated with tumors, is hypothesized to be caused by ochratoxins^{4,10}. Finally, fumonisins, the mycotoxin of interest for my thesis, are produced by various fungi from the *Fusarium* and *Aspergillus* genera and are toxic to the crops

they colonize, livestock that use these crops as feed, and to humans in high concentrations.

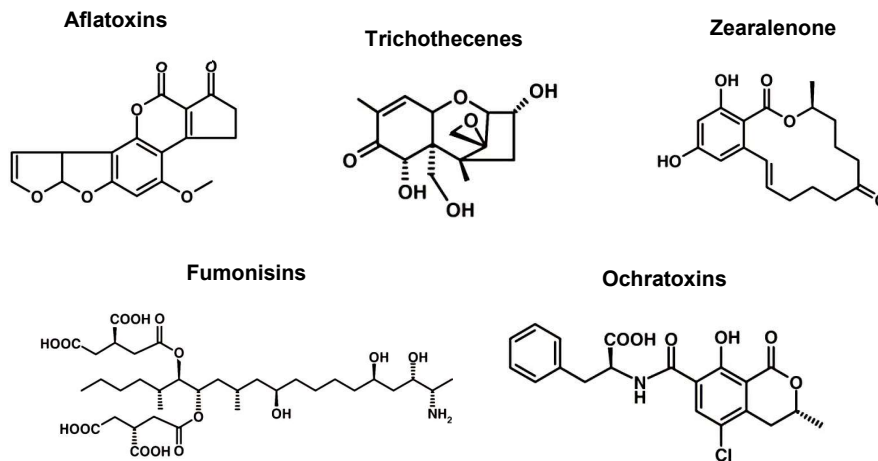


Figure 1. Chemical structures for the five main mycotoxin families. The most commonly studied mycotoxin from each family is shown as an illustration. The specific members of each family shown, from left to right, are aflatoxin B₁, fumonisin B₁ (FB₁), deoxynivalenol (DON), ochratoxin A (OTA), and zearalenone. Adapted from Richard (2007)⁴.

1.2 Fumonisin

1.2.1 *Fusarium* and *Aspergillus* spp. Fumonisin Production

Fumonisin mycotoxins are produced by *Fusarium* and *Aspergillus* spp.; primarily *F. verticillioides*, *F. proliferatum*, *F. moniliforme*, *A. niger*, and *A. welwitschiae*^{11,12}. In Canada and around the world, corn is the crop most affected, in addition to other cereals like wheat, barley, and rice¹³. Recent research has also shown that fumonisin contamination of wine grapes is becoming more common, especially from *Aspergilli* colonization^{14,15}. However, due to its prevalence and relatively high levels of fumonisin production, *F. verticillioides* presents the greatest risk for fumonisin poisoning. Moreover, *F. verticillioides* favours temperate and subtropical climates,

increasing the risk of fumonisin contamination in such areas, which also suggests that climate change may exacerbate fumonisin levels in the future¹⁶.

1.2.2 Fumonisin Structure and Toxicity

All the genes required for fumonisin biosynthesis, as well as transport and regulatory elements, are found on a single chromosome and referred to as a Fumonisin Biosynthetic Gene Cluster (BGC), which have been studied extensively in both *Fusaria* and *Aspergilli*^{17,18}. Many of the genes in each species' fumonisin BGC are highly conserved, however there are minor differences between protein homologs, and each have genes unique to their own BGC as well (e.g. FUM17 & 18 in *F. verticillioides*, and *sdr1* in *A. niger*) (Figure 2).

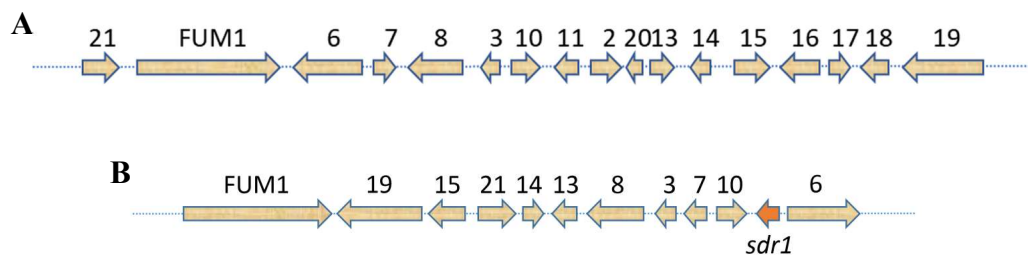


Figure 2. Schematic of fumonisin biosynthetic gene clusters (BGCs). Numbers represent “FUM” genes, whose products have unique roles in fumonisin biosynthesis and regulation. **A.** *F. verticillioides* fumonisin BGC. **B.** *A. niger* fumonisin BGC.

Overall, fumonisins are products of polyketide and amino acid metabolism^{19,20}. The B series (i.e. FB fumonisins) are the most common and are composed of an 18-carbon polyketide backbone with four main functional groups: an alanine-derived amine, two tricarballylic esters (TCEs), one to four hydroxyl groups, and two methyl groups (Figure 3)²¹. There are five main FB congeners that differ only in the number and position of the hydroxyl groups, with FB₁ being the most abundant and most

toxic, followed by FB₂₋₄, then FB₆. Less common fumonisins have also been identified, such as the *N*-acetylated A series (FA), as well as the C series (FC), which contain a shorter poly-carbon backbone^{22,23}. With regards to the B series, *Fusarium* spp. only produce FB₁₋₄ while *Aspergilli* produce FB₂, FB₄, and FB₆. Additionally, *Fusarium* spp. generally produce only FB fumonisins, whereas *Aspergilli* enzymatically convert their FB fumonisins to less toxic forms (see section 1.4). FB toxicity is mediated primarily by the amine group, in addition to the TCEs: varieties lacking the TCEs are significantly less toxic, and varieties lacking the amine are even less so^{24,25}. Fumonisins are sphingolipid analogs and disrupt their biosynthesis by competitive inhibition of ceramide synthase. It is thought that they bind to the enzyme's adjacent and contiguous sphinganine and fatty acyl-coenzyme A (CoA) binding sites via the amine and TCE functional groups, respectively. This results in the accumulation of sphinganine and other sphingoid bases, which can ultimately promote necrosis and carcinogenesis due to large disruptions in cell regulation and metabolism.

As such, fumonisins are associated with a number of negative health effects in both humans and animals, along with being harmful to host crops. They are phytotoxic, and the colonization of *Fusarium* spp. on corn crops leads to diseases like kernel rot as their fumonisins break down the plant matter²⁶. Without strict regulations, fumonisins could cause significant agro-economic losses due to their association with livestock mortality. They cause diseases such as equine leukoencephalomalacia and porcine pulmonary edema, which are commonly seen in farm animals that consume contaminated corn and dried distillers' grains and solubles (DDGS) as feed^{27,28}.

Fumonisins are also classified as a Group 2B carcinogen by the International Agency of

Research on Cancer (IARC), meaning they are possibly carcinogenic in humans, and are associated with increased incidences of esophageal cancer²⁹. They are also hepatotoxic and have been linked with the development of neural tube defects. These health issues are especially concerning in rural and developing communities where people are more likely to consume contaminated corn or other goods. To illustrate, the Transkei district of South Africa, where home-grown corn makes up a large part of the residents' diet, has one of the highest rates of fumonisin-contaminated corn in the world, previously reaching FB₁ levels of up to 117,520 ng/g³⁰. This region also experiences one of the highest global rates of esophageal cancer, suggesting FB₁ ingestion is the primary cause. Moreover, regions less than 200 km from Transkei without such high levels of fumonisin-contaminated corn experience relatively low rates of esophageal cancer, further implying a causal relationship with FB₁^{30,31}.

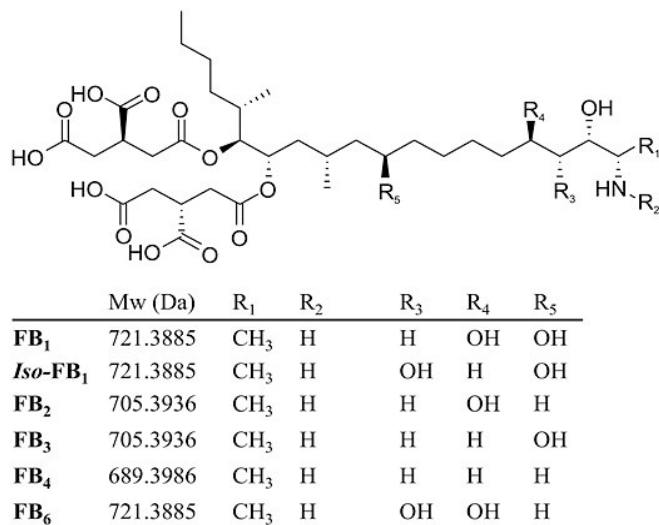


Figure 3. Structure of FB series fumonisins. The molecular weight and number/position of hydroxyl groups are depicted for all FB fumonisins. Adapted from Renaud *et al.* (2015)²¹.

1.3 Mycotoxin Prevention and Detoxification Strategies

Since mycotoxins are so prevalent not only in North America but around the world, numerous measures exist to combat the agro-economic and potential public health threats they pose; most of which are applied to fumonisin-implicated problems. These measures begin with good agricultural practices like early harvesting and proper drying of harvested goods to reduce fungal proliferation, with the goal of preventing mycotoxin contamination altogether^{2,32,33}. Biological control methods are also becoming more common, such as, for example, the development and introduction of non-pathogenic fungi to host crops to out-compete their mycotoxin-producing counterparts³⁴. To illustrate, a field study of the application of lab-generated, non-pathogenic strains of *A. flavus* and *A. parasiticus* to peanut crops resulted in a 95.9% decrease in aflatoxin contamination after harvesting³⁵. Moreover, traditional crop protection methods like pesticide use also remain popular: fungicides such as tebuconazole (Folicur[®]) and prochloraz (Sportak[®]) are often used to curtail *Fusarium* colonization on wheat, for example. In cases where mycotoxins have been ingested, adsorption agents are sometimes used. Specifically, certain clay minerals like calcium montmorillonite (NovaSil[™]) can sequester mycotoxins in animal and human gastrointestinal tracts^{2,36}. Clinical trials have suggested that this enterosorbent is the most selective and effective available: it has been shown to significantly reduce the harmful effects of aflatoxin poisoning while causing only mild side effects. However, enterosorbent use presents many potential risks as well, chief of which is their hinderance of essential nutrient absorption. Along with these prevention strategies, countries around the world have strict regulations on maximum mycotoxin levels in agricultural goods, ensuring any

consumption occurs in amounts significantly lower than necessary to cause adverse effects.

Although there is an abundance of strategies in place to deal with mycotoxin contamination, this is still a growing field that is being addressed from a number of perspectives. The drawbacks of the previously described methods, like the unsustainable nature of pesticide use and the health risks associated with adsorption agents, create the need for safer, more effective, and more sustainable alternatives. One of these is biotransformation; the enzymatic conversion of mycotoxins to less or non-toxic forms. A variety of microorganisms are capable of this conversion, and researchers are working to exploit this ability through recombinant enzyme technology³⁷. One example is the *Brevibacterium* species and its ability to break down compounds with characteristic hetero and polycyclic ring structures. In fact, it has been shown in the literature that various *Brevibacterium* species can completely degrade OTA at concentrations up to 40 mg/L, suggesting the presence of a carboxypeptidase enzyme that hydrolyzes the OTA amide bond, resulting in phenylalanine and the less toxic ochratoxin α (OT α)³⁸.

1.4 Fumonisin Toxicity Defense in *Fusaria* vs. *Aspergilli*

In addition to the diseases they cause in plants, animals, and humans, mycotoxins can also be toxic to the fungi that produce them. As such, certain species have evolved mechanisms to deal with this toxicity. One of these mechanisms is the expression of homologs of the mycotoxin's target protein. For example, *A. nidulans* express a proteasome subunit (inpE) to compensate for proteasome inhibition by the mycotoxin fellutamide B³⁹. Similarly to the bacterial biotransformation described above, some fungi resist the effects of their mycotoxins by post-biosynthetically modifying them

to reduce their toxicity. For example, there are reports of numerous *Rhizopus* spp. that degrade aflatoxin B₁ or convert it to less toxic forms^{37,40,41}. Researchers have also shown that some strains within this genus can fully degrade zearalenone, and others that hydrolyze OTA's amide bond^{37,42,43}. Importantly, fumonisin-producing *F. verticillioides*, *A. niger*, and *A. welwitschiae* also possess their own resistance mechanisms, some of which are discussed below. However, our understanding of how these systems work and how they evolved remains incomplete.

1.4.1 Fumonisin Poisoning Resistance in *Fusaria*

While it is unclear if their fumonisin resistance mechanisms evolved for the explicit purpose of self-protection, different genera protect themselves in separate ways. For example, *Fusaria* express proteins that compensate for the fumonisin-mediated inhibition of sphinganine biosynthesis. FUM17 and FUM18, two genes unique to the *F. verticillioides* fumonisin BGC, encode ceramide synthase enzymes; the protein that is competitively inhibited by FB fumonisins¹⁷. These enzymes have no role in fumonisin biosynthesis, confirmed via gene knockout studies, but are presumed to encode additional versions of the enzyme to compensate for FB-implicated inhibition of the native isoforms⁴⁴. This suggestion was confirmed for the FUM18 gene product, however further studies are required for FUM17. *F. verticillioides* FUM17 knockouts have not shown increased sensitivity to fumonisins, possibly due to the fact that *F. verticillioides* already contains three ceramide synthase genes outside its fumonisin BGC (CER1, CER2, and CER3)^{45,46}.

1.4.2 Post-Biosynthetic Fumonisin Detoxification in *Aspergilli*

As mentioned, certain species of *Aspergilli*, namely *A. niger* and *A. welwitschiae*, are capable of enzymatically converting their own FB fumonisins to less toxic forms, termed FPy and FLA (Figure 4)^{47,48}. These new forms were discovered when members of the Sumarah lab were monitoring for fumonisin and ochratoxin production by *Aspergilli* in Canadian vineyards. Since FB fumonisins are phytotoxic, Burgess *et al.* used a duckweed biomass assay to compare the toxicity of the deaminated FPy forms to their FB counterparts. They observed considerable growth inhibition and discolouration upon incubation with FB₁ and FB₄ at concentrations between 0.3-5.0 μM ⁴⁷. In contrast, concentrations of up to 40 μM were required to observe the same phytotoxic effects after incubation with FPy₁ and FPy₄.

When monitoring changes in fumonisin levels over a number of days in *A. welwitschiae* liquid culture, Burgess *et al.* also noted the presence of fumonisins with a terminal hydroxyl group (termed FLA) in addition to the FPy forms. Over the screening period, FB levels decreased markedly while FPy and FLA levels increased, although FLA amounts remained considerably lower than FPy for the duration of screening. Using the same duckweed assay, the toxicities of FLA₁ and FLA₄ were compared to their FPy counterparts. Again, concentrations of up to 40 μM were required for similar phytotoxic effects to the FB forms. However, at the same concentrations as FPy₁ and FPy₄, FLA₁ and FLA₄ appeared to inhibit duckweed growth to a lesser extent, suggesting the FLA forms are potentially even less toxic than the FPy forms.

Taking these results together led the Garnham and Sumarah labs to hypothesize that there is a sequential deamination of FB fumonisins to their FPy forms, followed by

reduction of the FPy carbonyl to the FLa hydroxyl. This eventually led to the identification and characterization of AnFAO (*A*spergillus niger Fumonisin Amine Oxidase), an enzyme responsible for the oxidative deamination of the FB amine to a ketone, giving the FPy form⁴⁸. However, the enzyme(s) responsible for the hypothesized FPy reduction remained unknown.

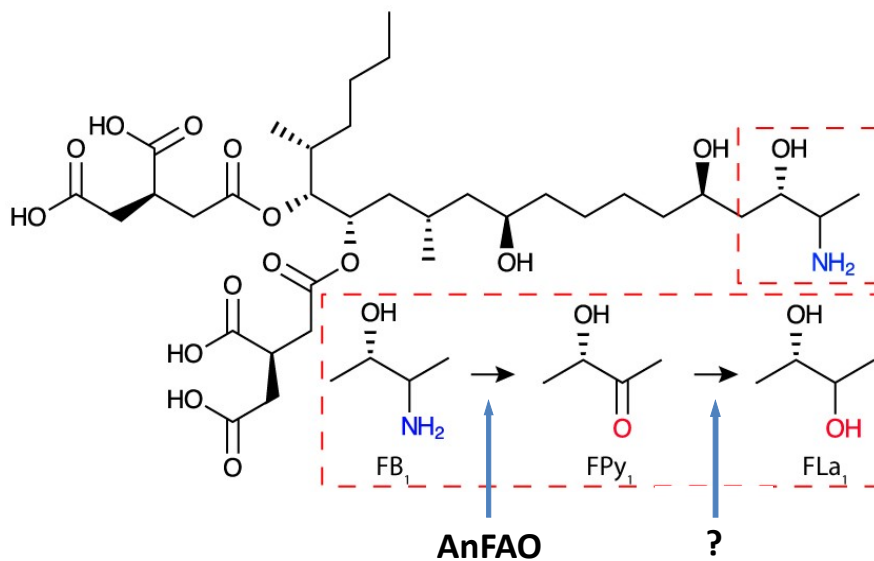


Figure 4. Enzymatic detoxification of FB₁. Shown is the deamination of the terminal amine on FB₁ to a carbonyl, resulting in FPy₁, followed by the (hypothesized) reduction of the FPy₁ carbonyl to a hydroxyl, resulting in FLA₁.

1.5 Experimental Approach and Objectives

The primary goal of my thesis was to identify the enzyme(s) responsible for generating FLa fumonisins. I utilized two distinct methodologies to do this: a discovery-based approach involving enzymatic enrichment from fungal cultures, and a hypothesis-based approach analyzing recombinant enzyme candidates hypothesized to be capable of reducing FPy fumonisins to FLa forms. Several in-house strains of *A. niger* and *A. welwitschiae* were grown in liquid culture with the goal of identifying those that generate

the most FLa fumonisins. Strains that produced the highest levels of these detoxified forms were used for subsequent biochemical enrichment experiments.

I was ultimately unable to enrich for and identify enzymes capable of FLa generation from any strain of *Aspergillus*. However, our recombinant enzyme studies indicated that FUM13, an oxidoreductase within the fumonisin BGC that is responsible for reduction of a ketone intermediate at position three of the fumonisin backbone⁴⁹, was capable of generating FLa fumonisins when administered FPy fumonisins as substrates. Both *A. niger* and *F. verticillioides* homologs of the enzyme were capable of performing this reaction, albeit very slowly. These results raised interesting questions regarding the ability of *F. verticillioides* to post-biosynthetically detoxify its own fumonisins in a similar manner to *A. niger* and *A. welwitschiae*. We therefore monitored for the ability of *F. verticillioides* to produce both FPy and FLa fumonisins via LC-MS. While the majority of strains did not produce either of the detoxified congeners, a select few were capable of their generation. Additional bioinformatic analysis identified a close homolog of AnFAO within *F. verticillioides*. Recombinant expression and biochemical characterization of this enzyme (termed FvFAO – *Fusarium verticillioides* **F**umonisin **A**mine **O**xidase) indicated that it was capable of generating FPy fumonisins, but at a reduced rate compared to AnFAO. Overall, my thesis reports for the first time an enzyme capable of generating FLa fumonisins *in vitro* (FUM13), as well as the production of FPy and FLa fumonisins by specific strains of *F. verticillioides*. Finally, recombinant production of AnFAO's closest homolog within *F. verticillioides* (FvFAO) revealed that it is capable of generating FPy fumonisins *in vitro*.

Chapter 2 – Materials and Methods

Many methods described below appear in, or are adapted from, Shane Butler's MSc thesis, a former graduate student in the Garnham lab⁷².

2.1 LC-MS Screening of Fungal Culture Supernatants

For FLA fumonisin screening, 14 strains of *A. niger* and *A. welwitschiae* were grown in 200 mL of YES media in Roux flasks. Each strain was transferred from YES agar plates to liquid culture after mechanical homogenization, and then grown at 30°C for 8 weeks. Samples of culture supernatant were taken once a week and prepared for LC-MS analysis by diluting 10-fold with 60% methanol before high-speed centrifugation.

For strains whose culture supernatants were concentrated for FLA-generating enzyme enrichment experiments, either 75% or 90% w:v ammonium sulfate was used to precipitate ~200 mL of supernatant. The precipitates were pelleted by centrifugation at 20,000g/4°C for 20 minutes before resuspension in 2-5 mL of AMS Buffer 1 (50 mM Tris, pH 8.0, 150 mM NaCl) or AMS Buffer 2 (50 mM MES, pH 6.0, 150 mM NaCl). Resuspended and concentrated supernatants were dialyzed exhaustively at 4°C against 1 L of AMS Buffer 1 or AMS Buffer 2 to remove excess ammonium sulfate, resulting in volume increases to 10-20 mL.

The *F. verticillioides* strain discussed in Figure 26 was grown by Megan Kelman, a technician in the Sumarah lab. The fungus was grown in 200 mL of modified MYRO media ((NH₄)₂HPO₄ (1 g), KH₂PO₄ (3 g), MgSO₄-7H₂O (0.2 g), NaCl (5 g), sucrose (40 g), and glycerol (10 g) per L ddH₂O) in a Roux flask. It was transferred from MEA plates to liquid culture and then grown at 25°C for 6 weeks. Culture supernatants

were completely evaporated then resuspended in 1 mL modified MYRO media before screening by mass spectrometry.

LC-MS analysis was performed using an Agilent 1290 HPLC system coupled to a Q-Exactive Quadrupole Orbitrap mass spectrometer (Thermo Scientific). 5 μ L of the reaction mixtures were injected onto an Eclipse Plus C18 RRHD column (2.1 \times 50 mm, 1.8 μ m; Agilent Technologies) maintained at 35°C and operating at 0.3 mL/min. Compounds were resolved using a gradient program consisting of water with 0.1% formic acid (mobile phase A), and acetonitrile with 0.1% formic acid (mobile phase B) (Optima grade, Fisher Scientific). Mobile phase B was held at 0% for 0.5 min before increasing to 100% over 3.5 min, held at 100% for 2.5 min, before returning to 0% over 0.5 min. Heated electrospray ionization (HESI) was operated in negative ionization mode with the following settings: temperature, 400°C; sheath gas, 17 units; auxiliary gas, 8 units; probe heater temperature, 450°C; S-Lens RF level, 45.00. The capillary voltage was 3.5 kV for negative ionization. The MS data were acquired using non-targeted DDA that included a full MS scan at 35000 resolution, with a scan range of 600–800 m/z ; automatic gain control (AGC) target, 3×10^6 and a maximum injection time (max IT) of 128 ms. The five highest intensity ions were selected from each full scan for MS/MS analysis using a 1.2 Da isolation window, and were analyzed using the following conditions: resolution, 17500; AGC target, 1×10^6 ; max 17 IT, 64 ms; normalized collision energy, 35; intensity threshold, 1.5×10^5 ; dynamic exclusion, 5 s. Data were analyzed using the Xcalibur software package. Fumonisin analytes were confidently detected at a mass accuracy of 3 ppm, retention time matching those of standards at ± 0.05

min. All fumonisins were also identified by the characteristic product anion $C_6H_5O_5^-$ of the $[M-H]^-$ molecular ion in MS/MS²¹.

2.2 FPy Synthesis

FPy₁, FPy₂ and ¹³C-labeled FPy₂ (¹³C-FPy₂) were synthesized to be used as substrates for FLa-generating enzyme candidates. Varying concentrations of FB₁, FB₂, and ¹³C-FB₂ stored in either DMSO, methanol, or acetonitrile were completely dried before each reaction. AnFAO was added to phosphate-buffered saline (PBS), pH 7.2 at a concentration of 3 μM in each reaction, along with 8.5 nM catalase. Reactions were incubated overnight (16-24 h) at 37°C in a thermal shaker at 300 rpm. The solution was then diluted with water and pH adjusted to 2.2 with concentrated HCl. 2x volume (~4 mL) of ethyl acetate was added, vortexed, and fumonisins were extracted from the organic layer after phase separation. This process was performed twice to ensure complete fumonisin extraction. The organic phase was dried before resuspending the fumonisins in 75-100% acetonitrile. Reaction completion was verified each time by LC-MS using an Agilent 1290 HPLC system coupled to a Q-Exactive Quadrupole Orbitrap mass spectrometer (Thermo Scientific) in the same manner as discussed in section 2.1.

2.3 Reverse-Phase Fumonisin Extraction

6 cc Oasis HLB cartridges (Waters™) containing a polymeric reversed-phase sorbent can be used for the extraction of acidic, basic, and neutral compounds from complex solutions with a pH range between 0-14. These cartridges were used for the extraction of fumonisins from solid mycelia in order to reduce LC-MS background signals and filter the samples before injection onto the mass spectrometer.

Cartridges were activated with 2 column volumes (CVs) of 100% methanol before conditioning with 2 CVs of ddH₂O and pH adjusting to 2.0. Samples were generously diluted with ddH₂O, pH 2.0 (ddH₂O was pH adjusted with concentrated HCl) and loaded onto the columns. 2 mL washes were performed with 25%, 50%, 75%, and 100% methanol. Samples from each wash were analyzed on a Q-Exactive Quadrupole Orbitrap mass spectrometer (Thermo Scientific) to determine which methanol percentage each fumonisin elutes at. No fumonisins eluted before the 75% methanol wash, therefore up to 50% methanol can be used to wash the HLB columns before eluting fumonisins.

2.4 Fungal Protoplast Preparation & Assays

Fungi were inoculated on YES plates from agar plugs stored at 4°C and allowed to reach 100% confluency at 30°C. 5-10 mL YPD media was added to the plate, and a sterile toothpick was used to transfer mycelia to an Erlenmeyer flask with 100-200 mL YPD media. The fungi were allowed to grow for ~3 weeks at 30°C before transferring the entire mycelial mat to a funnel protected with sterile 22-25 µm Miracloth. 200 mL of 0.6 M MgSO₄ was used to wash away fungal spores before transferring ≤ 2 g of mycelia to sterile 50 mL tubes. 10 mL of a filter-sterilized mixture of 8 mg/mL β-D glucanase, 5 mg/mL driselase, and 80 U/mL lyticase in 1.1 M KCl, 0.1 M citric acid, pH 5.8 was added to each tube of mycelia then allowed to incubate at 37°C/120-150 rpm for 4 hours. The resulting mixture was filtered with Miracloth and transferred to a new sterile tube, then centrifuged at 1000g for 10 minutes. The supernatant was removed and the protoplast pellet was washed twice with 10 mL 1.2 M sorbitol, 50 mM Tris, pH 7.5 and centrifuged at 1000g. The washed protoplasts were then resuspended at 0.5 mL/g of starting mycelia in either a 1:1 mixture of 1.2 M sorbitol, 50 mM Tris, pH 7.5:YPDS (if

they were to be left intact), or in 50 mM Tris, pH 8.0, 150 mM NaCl, 1 mM DTT, 10% glycerol (if they were to be lysed by sonication).

Reactions were performed by incubating intact or sonicated protoplast samples with either 2.8 μM FB₁, 2.8 μM FPy₁, 0.28 μM ¹³C-FB₂, or 0.28 μM ¹³C-FPy₂ at 37°C, with shaking, for a period of 4 days. Samples were diluted 10-fold with 60% methanol, then diluted 2-fold further with 100% methanol before analysis by LC-MS. Relative fumonisin amounts were determined via LC-MS using an Agilent 1290 HPLC system coupled to a Q-Exactive Quadrupole Orbitrap mass spectrometer (Thermo Scientific) in the same manner as discussed in section 2.1.

2.5 Expression Vectors

2.5.1 Construct Design and Engineering

Constructs were designed based on secondary structure predictions for each protein of interests' amino acid sequence as determined by Phyre², a secondary structure and homology modeling software⁷³. Regions predicted to fold into a transmembrane helix with moderate to high confidence were eliminated from each construct by the introduction of a premature stop codon, resulting in C-terminal truncations of varying lengths.

2.5.2 Cloning and Vectors

Genes for FvFAO, sdr1, *A. niger* FUM13, and *F. verticillioides* FUM13 variants were either synthesized by TWIST Bioscience or cloned via ligation independent cloning (LIC) or Gateway[®] technology following protocols provided by Addgene and Invitrogen, respectively. Each gene was synthesized in or cloned into one of 3 vectors: a pET His6

TEV LIC cloning vector that contains a Tobacco Etch Virus (TEV)-protease cleavable 6x-His-tag (His6) at the N-terminus of the protein (Addgene plasmid #29656, a gift from Scott Gradia), or the same vector with either a maltose-binding protein (MBP) or Glutathione S-transferase (GST) solubility tag at the N-terminus.

2.5.3 Site-Directed Mutagenesis

Mutagenesis was performed using a QuickChange Site-Directed Mutagenesis Kit from Agilent Technologies with the protocol provided. Primers were designed based on the instruction manual guidelines. Resulting clones were verified by sequencing performed by Eurofins Genomics or the Robarts Research Institute.

2.6 Protein Expression and Purification

2.6.1 Protein Expression

Each protein was expressed in BL21 (DE3) *E. coli* (Invitrogen). Cells were grown in Terrific Broth (TB) media at 37°C to an OD₆₀₀ of 0.5-0.9 before induction with 0.1-1 mM isopropyl β-D-1-thiogalactopyranoside (IPTG) and 0-5% v/v ethanol. Induction occurred overnight (16-20 h) with shaking at 25°C before harvesting by centrifugation: cells were centrifuged at 4000 rpm/18°C for 15 minutes. Cells containing constructs with *sdr1*, *A. niger* FUM13, or *F. verticillioides* FUM13 variants were resuspended in NiA buffer (50 mM Tris, pH 8.0, 500 mM NaCl, 5 mM β-mercaptoethanol, 10 mM imidazole) with protease inhibitors. Cells containing FvFAO constructs were resuspended in NiA2 buffer (50 mM MES, pH 6.0, 500 mM NaCl, 5 mM β-mercaptoethanol, 10 mM imidazole) with protease inhibitors.

2.6.2 Protein Purification

Cells were lysed with a Q Sonic 500 Series sonicator (amplitude: 30%, time on: 30 s, time off: 30 s) for 6 minutes, and the lysates were clarified by centrifugation at 20,000g/4°C for 1 hour. The clarified lysate was loaded onto a 1 mL or 5 mL HisTrap HP nickel-chelating column (Cytiva) equilibrated with either NiA or NiA2 buffer. The column was then washed with 15 column volumes (CVs) of NiA/NiA2 buffer, followed by another 15 CV wash with NiA/NiA2 buffer containing 25 mM imidazole. Each protein was eluted with 2 CVs of NiB/NiB2 buffer (NiA/NiA2 with 300 mM imidazole) unless otherwise indicated in Chapter 3. This was followed by either exhaustive dialysis at 4°C against 1 L of NiA/NiA2 buffer with 50 mM NaCl, or size-exclusion chromatography. Size-exclusion chromatography was performed using a Bio-Rad ENrich™ SEC 650 or Superdex 200 10/300 GL (GE Healthcare) column equilibrated with either SEC-A buffer (50 mM Tris, pH 8.0, 50 mM NaCl) or SEC-A2 buffer (50 mM MES, pH 6.0, 150 mM NaCl). Fractions containing the protein of interest were pooled, concentrated with a centrifugal concentrator (MWCO = 10 kDa or 30 kDa), and their concentration determined by a Bradford Assay. Each protein was then used immediately for enzyme assays, or flash frozen in liquid nitrogen after the addition of 5-10% v/v glycerol and stored at -80°C until further use.

2.7 LC-MS Detection of Enzymatically Modified Fumonisin

LC-MS fumonisin deamination and reduction assays were performed in 1.5 mL microcentrifuge tubes. Reactions were performed in SEC-A buffer for FLA-generating assays, and SEC-A2 buffer for FB-deaminating assays. Fumonisin concentrations in each reaction ranged between ~0.5-110 µM, and NADPH cofactors

were included at 50 μM for the FLa-generating assays. After each reaction, samples were diluted with varying concentrations of methanol (60-100%) depending on the reaction volume. Final methanol concentrations in each sample before injecting onto the mass spectrometer were greater than or equal to 50%. Fumonisin concentrations were standardized to ~ 0.1 ppm (relative to the initial concentration of each substrate added) via the methanol dilutions before sample injection.

LC-MS analysis was performed using an Agilent 1290 HPLC system coupled to a Q-Exactive Quadrupole Orbitrap mass spectrometer (Thermo Scientific) in the same manner as discussed in section 2.1.

2.8 AmplexTM Red Relative Rate and Kinetic Assays

Reactions were performed in triplicate in a 96-well plate consisting of a solution with 50 mM Tris, pH 8.0, 150 mM NaCl, 200 μM AmplexTM Red, 2 U/mL horseradish peroxidase (HRP), and substrate (100 μM for FB₁ and FB₂ relative rates, 50 μM for sphinganine relative rates, 25 μM - 2.5 mM for FB₁ kinetics, and 10 μM - 500 μM for sphinganine kinetics). Enzyme concentrations ranged from 20-100 nM depending on substrate being tested and the type of assay being performed. H₂O₂ reacts with AmplexTM Red (1:1) in the presence of HRP to produce resorufin, which absorbs at 571 nm, allowing rates to be determined using an H₂O₂ standard curve. The standard curve was generated using H₂O₂ at concentrations of 0.3125 μM , 0.625 μM , 1.25 μM , 2.5 μM , and 5 μM mixed 1:1 with 50 mM Tris, pH 8.0, 150 mM NaCl, 200 μM AmplexTM Red, and 2 U/mL horseradish peroxidase (HRP). Reactions were incubated for 30 minutes at 37°C with absorbance measured at 571 nm every 3 minutes. For relative rate assays, initial rates in the linear range were measured in triplicate for each enzyme at the same substrate

concentration. For kinetic assays, initial rates at increasing substrate concentrations were measured in triplicate to determine Michaelis-Menten parameters of FvFAO for FB₁ and sphinganine substrates. K_M and k_{cat} values for each substrate were calculated in SigmaPlot using the Michaelis-Menten nonlinear curve fitting model.

Chapter 3 – Results

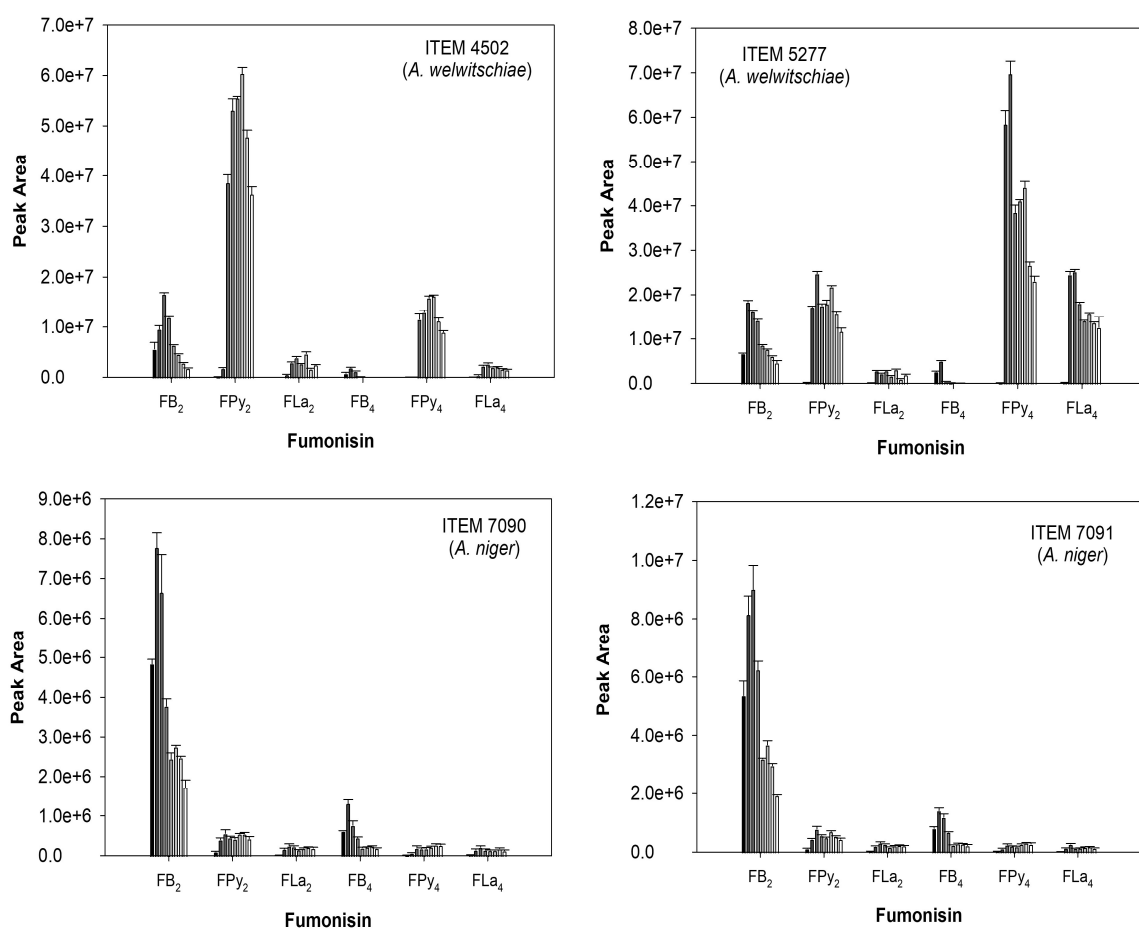
3.1 Fungal Culture Fumonisin Screening

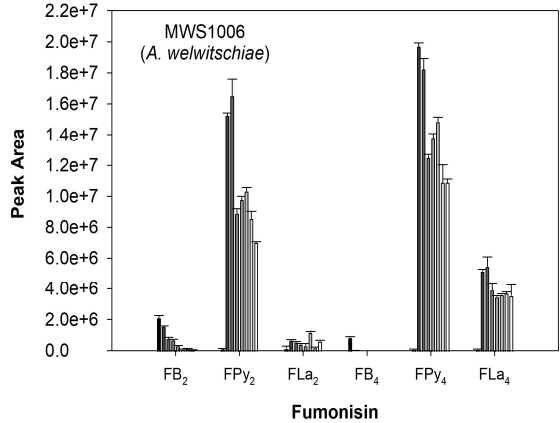
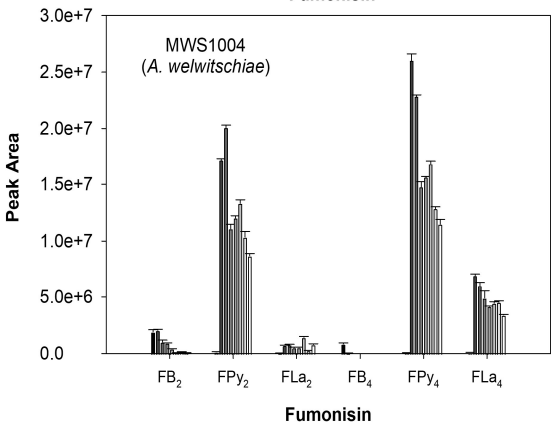
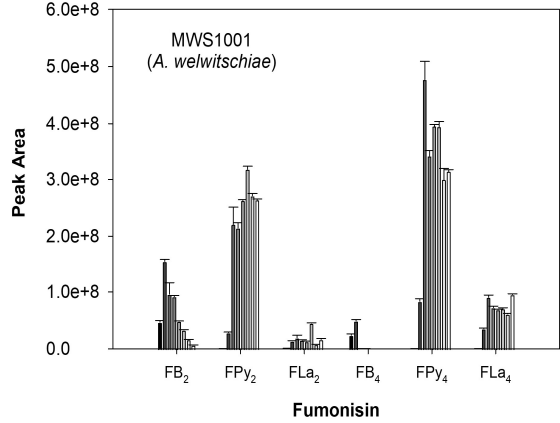
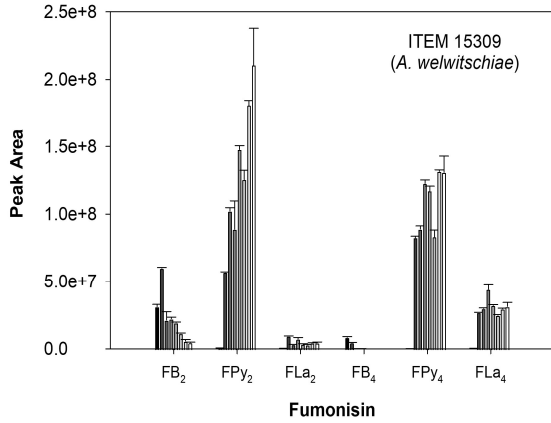
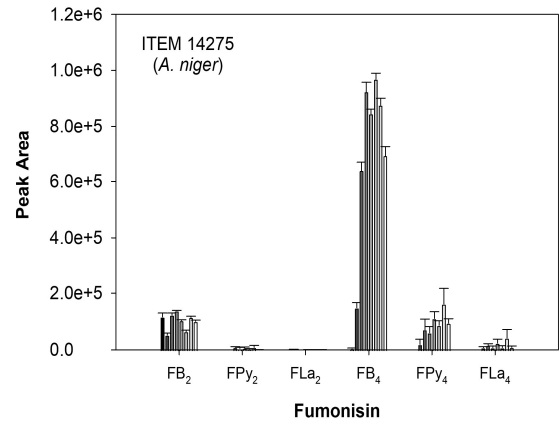
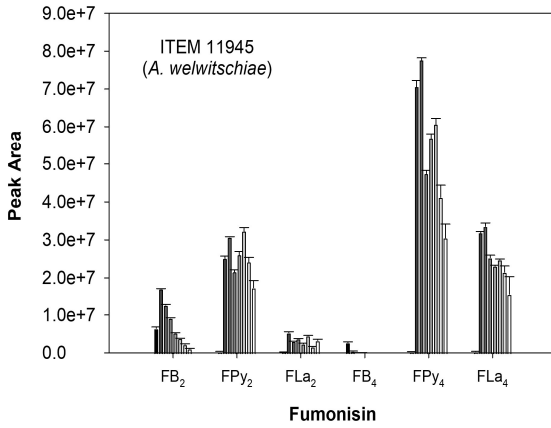
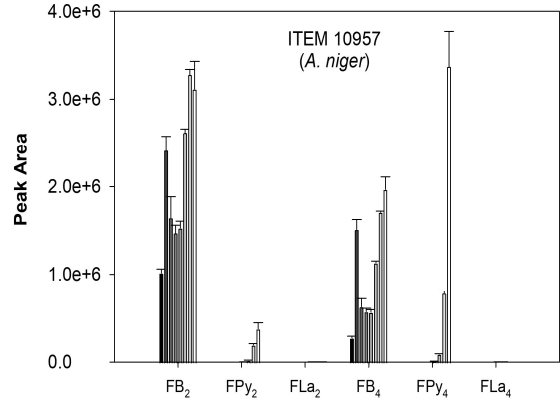
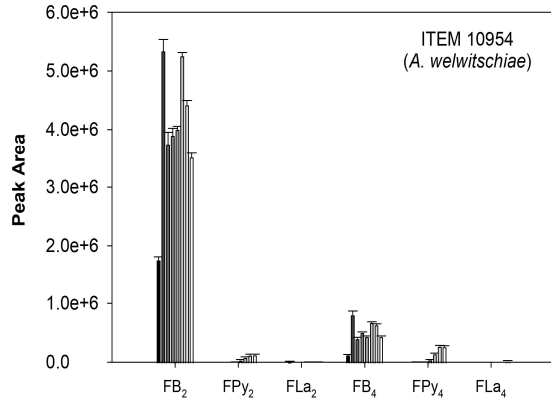
Fumonisin production by 14 in-house strains of *A. niger* and *A. welwitschiae* was monitored for 8 weeks to identify strains with the greatest FLA-producing activity. Samples of culture supernatant were isolated once a week and analyzed by LC-MS. High-producing strains were then used for enzyme identification experiments. Fumonisin levels, as determined by LC-MS peak area, are depicted in Figure 5. Peak areas were used as a measure of abundance for several mass spectrometry figures in this thesis since many fumonisins are not commercially available or are cost prohibitive. Therefore, we were unable to obtain standards to measure their absolute concentrations. Although there are some differences in ionization efficiency between fumonisins, operating the mass spectrometer in negative ionization mode mitigates these differences since they each contain two TCE sidechains that are responsible for deprotonation.

Relative amounts are only shown for the 2 and 4 series fumonisins; the 6 series were produced in much lower quantities and omitted. Fumonisin levels varied greatly between strains, with some producing little to no FPy or FLA forms (e.g. ITEM 10954, ITEM 10957, DNA239). Some strains produced more 2 series fumonisins than 4 (e.g. ITEM 4502), while others produced more 4 series fumonisins than 2 (e.g. MWS1004). Moreover, most strains that produced high levels of the post-biosynthetically generated forms made more FPy₄ and FLA₄ than FPy₂ and FLA₂, respectively. These strains include ITEM 4502, ITEM 5277, ITEM 11945, ITEM 15309, MWS1001, MWS1004, and MWS1006; all of which are *A. welwitschiae*. FPy₂ and FPy₄ were the most abundant for each of these strains over most timepoints, likely due to efficient deamination of FB₂ and

FB₄⁴⁸. In general, the *A. welwitschiae* strains produced more fumonisins than the *A. niger* strains. This is especially true for the post-biosynthetically generated forms; most of the *A. niger* strains produced very little to no FPY₂, FLA₂, FPY₄, or FLA₄.

Overall, MWS1001 was the greatest producer of FB, FPY, and FLA fumonisins, with peak areas in the 10⁷-10⁸ range. In comparison, ITEM 10954 was one of the worst fumonisin producers; FB₂ was only detected at peak areas reaching approximately 5.5×10⁶ for this strain, while no other form exceeded 1.0×10⁶. This strain also produced only trace amounts of FLA₂ and FLA₄, with none detected on some weeks.





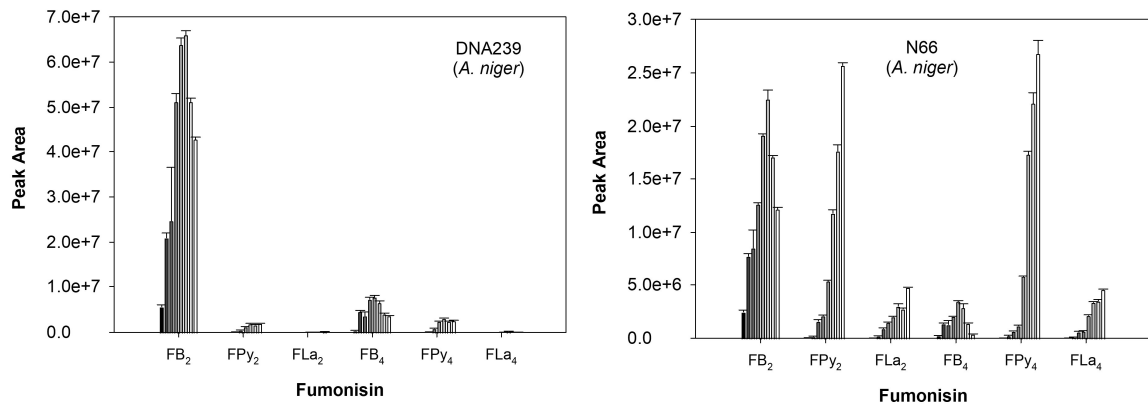


Figure 5. Abundance of the 2 and 4 series fumonisins in 14 strains of *A. niger* and *A. welwitschiae* culture supernatants. Fungi were inoculated in YES media and grown for a period of 8 weeks. Fumonisins amounts from each strain are illustrated by LC-MS peak area. Peak areas are the means \pm SEM of 3 biological replicates. Weekly data is shown in grayscale from black (1 week) to white (8 weeks). Strains with the prefix “ITEM” originated in Italy, and strains with the prefixes “MWS”, “N”, and “DNA” originated in Canada.

Figure 6 shows the change in FLA₂ and FLA₄ levels over 8 weeks for the seven highest FLA-producing strains, with most peaking between 2-4 weeks. FLA₂ levels are comparable for six of the seven strains (Figure 6A), however, ITEM 5277, ITEM 11945, and ITEM 15309 produced FLA₄ at levels nearly one order of magnitude greater than ITEM 4502, MWS1004, and MWS1006 (Figure 6B & C). Additionally, MWS1001 produced considerably more FLA₂ and FLA₄ over the 8 week period than each of the other six strains (Figure 6D). For example, MWS1001 peak areas for FLA₄ reached approximately 9.0×10^7 at 3 weeks, while the maximum FLA₄ peak area for the other six strains reached only half this value (4.5×10^7 – ITEM 15309 at 4 weeks).

FLA₂ and FLA₄ amounts for six of these seven strains are shown at weeks 2, 3, and 4 in Figure 7. While most produced considerable amounts of FLA₂, they all produced greater amounts of FLA₄, excluding ITEM 4502. Data is shown for weeks 2-4 since FLA levels peaked in this range for almost all strains, as previously mentioned. As well, this

time span is generally when *Aspergilli* metabolism is at its highest in liquid culture before slowing as the fungi begin to die. Considering these data, MWS1001 and ITEM 11945 were chosen as source material for biochemical enrichment of FLA-generating enzymatic activity. All experiments were performed with fungi that were growing in liquid culture for 3 weeks.

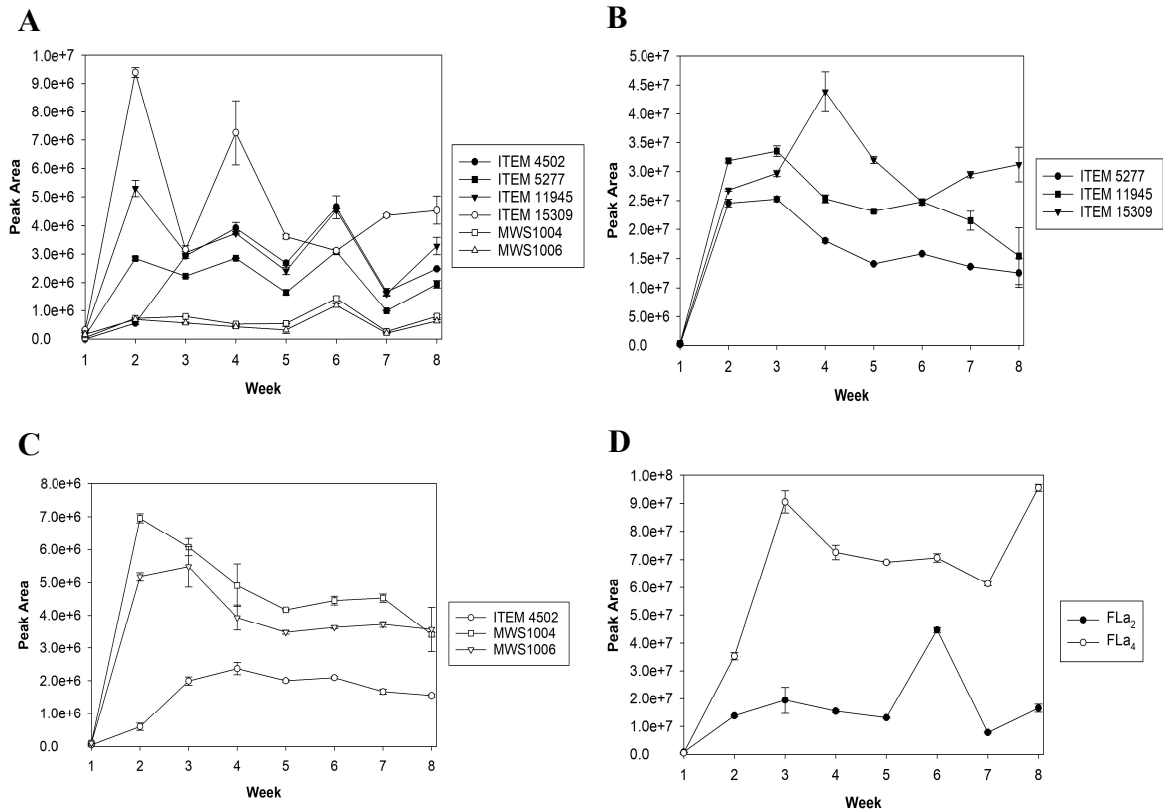


Figure 6. Change in FLA₂ and FLA₄ levels in culture supernatants over an 8 week period for the seven highest FLA-producing strains of *Aspergilli*. Fungi were inoculated in YES media and grown for a period of 8 weeks. Fumonisin amounts from each strain are illustrated by LC-MS peak area. Peak areas are the means \pm SEM of 3 biological replicates. **A.** FLA₂ levels from each strain, excluding MWS1001. **B.** FLA₄ levels from ITEM 5277, ITEM 11945, and ITEM 15309. **C.** FLA₄ levels from ITEM 4502, MWS1004, MWS1006. **D.** FLA₂ and FLA₄ levels from MWS1001.

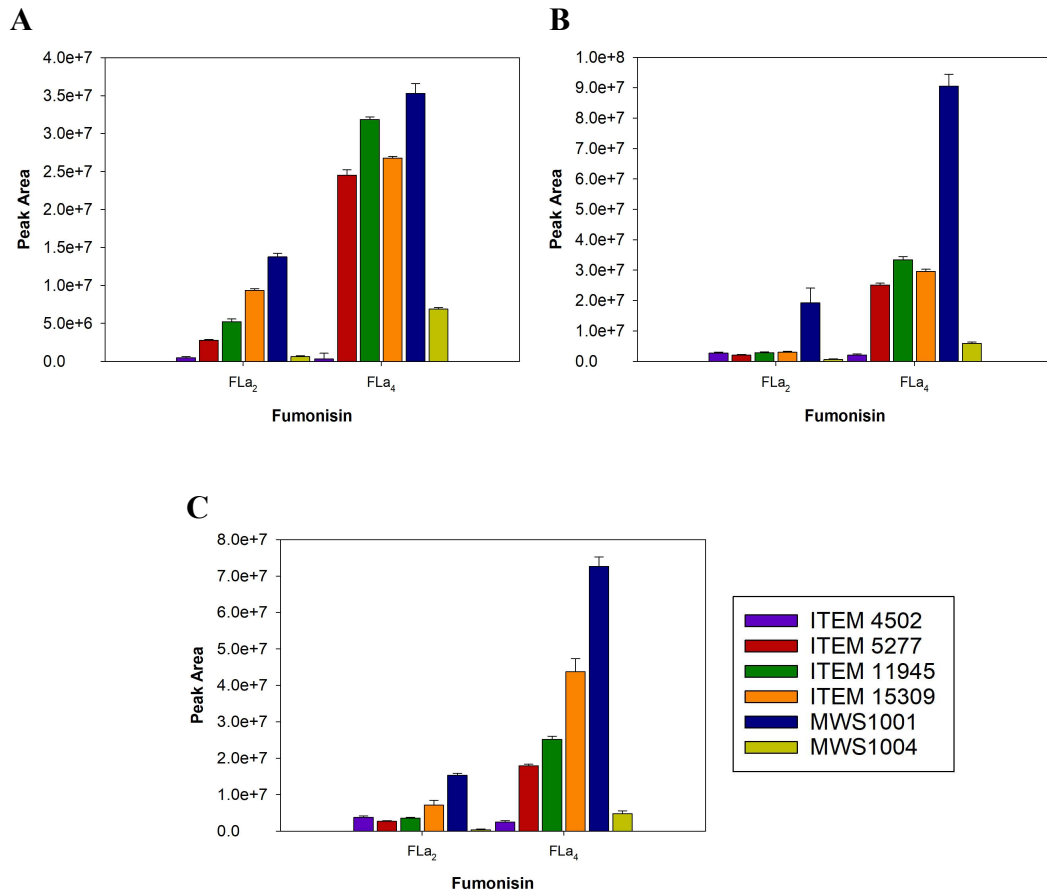


Figure 7. Abundance of FLa₂ and FLa₄ in culture supernatants after 2, 3, and 4 weeks for the six highest FLa-producing strains of *Aspergilli*. Fungi were inoculated in YES media and grown for a period of 8 weeks. Fumonisin amounts from each strain are illustrated by LC-MS peak area. Peak areas are the means \pm SEM of 3 biological replicates. FLa₂ and FLa₄ levels are shown for each strain at **A**. 2 weeks, **B**. 3 weeks, and **C**. 4 weeks.

We initially set out to follow the same workflow used for the discovery of AnFAO to identify the FLa-generating enzyme(s) that we hypothesized were also present in culture supernatants. AnFAO was identified via enrichment of FB-deaminating activity from this material using a series of traditional purification techniques: culture supernatants were simplified and concentrated via an ammonium sulfate precipitation before monitoring for FB deamination by LC-MS. Active fractions from each purification step were pooled before eventually identifying the enzyme by MS/MS proteomics⁴⁸.

Again, MWS1001 and ITEM 11945 were used for the following FLa-generating enzyme enrichment experiments. Two trials were performed for each strain. For the first trials, culture supernatants were precipitated with 75% w:v ammonium sulfate before pelleting by high-speed centrifugation. These pellets were resuspended in 2-5 mL AMS Buffer 1 (Tris, pH 8.0 – see section 2.1 for buffer components), then dialyzed exhaustively against the same buffer to remove excess ammonium sulfate. The same process was followed for the second trials with two differences: 90% w:v ammonium sulfate was used to precipitate the culture supernatants, and AMS Buffer 2 (MES, pH 6.0 – see section 2.1 for buffer components) was used instead of AMS Buffer 1. Final volumes after dialysis ranged between 10-20 mL, resulting in a 10-20 fold increase in protein concentration (i.e. 200 mL initial volume).

These concentrated and dialyzed supernatants were then incubated with $\sim 0.3 \mu\text{M}$ FB₁ or ¹³C-FB₂. ¹³C-labeled 2 series fumonisins (¹³C-FB₂, ¹³C-FPy₂, & ¹³C-FLa₂) were used in fungal experiments to differentiate from the 2 series congeners naturally produced by *Aspergillus* spp. (*Aspergilli* do not produce 1 series fumonisins). Multiple potential cofactor conditions were also tested separately for each strain: 10 μM NADH, 10 μM NADPH, 10 μM of both NADH & NADPH, MWS1001 or ITEM 11945 culture supernatant before precipitation (final concentration in the reaction was a 10-fold dilution), or no cofactor. NADH and NADPH were included since we hypothesized that the FLa-generating enzyme(s) are part of the SDR superfamily, which often use NAD(P)H cofactors to catalyze oxidoreduction reactions⁵⁰. Diluted culture supernatants were also used in case any unknown cofactors were present here before ammonium

sulfate precipitation. Reactions were performed overnight (16-20 h) in triplicate at room temperature and 37°C.

After analyzing all reactions by LC-MS, no FLa generation was observed (data not shown). These results suggested that the enzyme(s) responsible for FLa production are not present in culture supernatants. As such, I worked to analyze the conversion of exogenous fumonisin substrates by fungal cultures in an alternative manner (section 3.2).

3.2 FLa Production by *A. welwitschiae* Protoplasts

Since we observed no FLa generation in concentrated culture supernatants, we hypothesized that the FLa-generating enzyme(s) are potentially intracellular. Therefore, we investigated whether sonicated fungal cultures were capable of converting exogenous fumonisin substrates to FLa forms. First, small samples of solid fungal mycelia from MWS1001 and ITEM 11945 were isolated for sonication after growing for 3-4 weeks. Assays were performed by adding ~0.3 μM FB₁ and ¹³C-FB₂ to these sonicated mycelia, along with AnFAO in an effort to increase the amount of FPy fumonisins present in the mixture. Reactions were carried out overnight (16-20 h) at room temperature and 37°C, however no FLa generation was observed for any of the reaction conditions (data not shown).

In order to more effectively lyse the cells and monitor the presumed intracellular FLa-generating activity, we incubated MWS1001 mycelia with a mixture of cell wall-lysing enzymes to generate protoplasts before sonication once again. The protoplasts were sonicated and clarified by high-speed centrifugation before incubating the soluble

fraction with $\sim 0.3 \mu\text{M}$ $^{13}\text{C-FB}_2$, as well as $\sim 0.3 \mu\text{M}$ $^{13}\text{C-FPy}_2$ synthesized in the lab with AnFAO (note: no reactions were performed for lysed cells with FB_1 or FPy_1 substrates due to the limited amount of protoplasts that were generated). $50 \mu\text{M}$ NADPH was also included as a potential cofactor. However, after incubation at 37°C for 4 days, we observed little to no FLa generation for $^{13}\text{C-FB}_2$ (data not shown) or $^{13}\text{C-FPy}_2$ substrates (Figure 8).

Given these results, we also decided to investigate whether intact protoplasts were capable of converting added fumonisin substrates to FLa forms. Similar to the sonicated cells, these protoplasts were incubated separately with the same concentrations of FB_1 , $^{13}\text{C-FB}_2$, FPy_1 , and $^{13}\text{C-FPy}_2$ at 37°C for 4 days. Little to no FLa fumonisins were produced when FB_1 and $^{13}\text{C-FB}_2$ were added (data not shown). However, the protoplasts partially converted both FPy_1 and $^{13}\text{C-FPy}_2$ to their FLa forms over the reaction period (Figure 8). After incubation with FPy_1 , there was an almost 10% conversion to FLa_1 , while conversion of $^{13}\text{C-FPy}_2$ to $^{13}\text{C-FLa}_2$ exceeded 22%.

Although conversion was incomplete, this data suggests that FLa-generating enzymes from this fungus use FPy fumonisins as substrates, rather than FB forms. It is not entirely clear why we were able to observe FLa production by intact protoplasts, however if the FLa-generating enzyme(s) are membrane-associated or compartmentalized in the cell, then removing the cell wall may have led to easier substrate access without potential disruption from sonication. Importantly, this is the first time FLa production has been observed after the addition of exogenous fumonisin substrates to fungal cultures. More specifically, it is the first observation of ^{13}C -labeled FLa_2 by mass spectrometry.

These observations provide further evidence to support our hypothesis that FLa fumonisins are generated enzymatically via the reduction of FPy substrates.

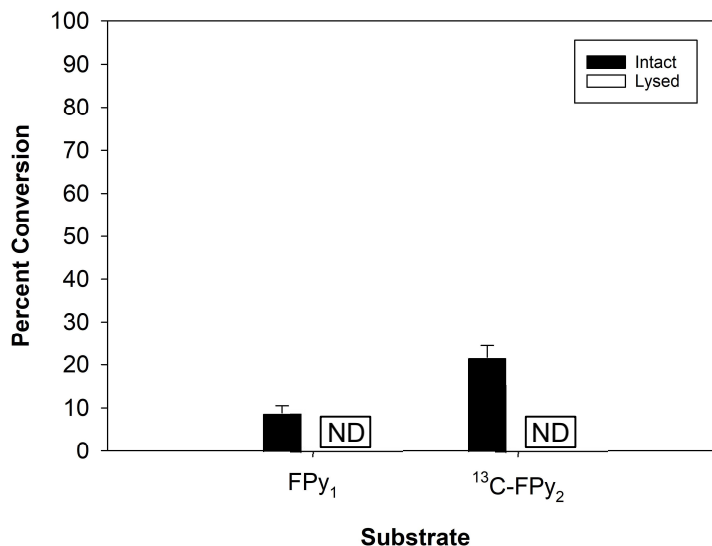


Figure 8. FLa₁ and ¹³C-FLa₂ generation by *A. welwitschiae* MWS1001 protoplasts. Fumonisin amounts are illustrated by the percent conversion of FPy substrates to FLa forms. Percentages are the means ± SEM of 3 biological replicates. Note: no reactions were performed for lysed protoplasts with FPy₁ as a substrate. “ND” denotes no detection of FLa fumonisins for the lysed protoplast reactions.

3.3 Analysis of FLa-Generating Enzyme Candidates

While MWS1001 protoplasts provided reliable FLa generation data, biochemical enrichment of FPy-reducing activity from this source material was not feasible (see section 4.1). Therefore, I shifted my primary research focus to the hypothesis-based approach where enzyme candidates were identified from the literature, then expressed and purified before assaying for FLa-generating activity *in vitro*.

A number of constructs were expressed before purification attempts with varying degrees of success. We focused on two candidate enzymes: 1) *sdr1*, a short-chain dehydrogenase/reductase (SDR) enzyme of unknown function present within the

fumonisin biosynthetic gene cluster of *Aspergilli*, and 2) FUM13, an NADPH-dependent oxidoreductase present within the fumonisin biosynthetic gene clusters of both *Fusarium* and *Aspergillus* spp. that is responsible for the reduction of a ketone intermediate to a hydroxyl on position 3 of the fumonisin backbone during biosynthesis⁴⁹.

3.3.1 *A. niger* sdr1

The *A. niger* sdr1 gene was identified, and the sequence generously provided, by Dr. Robert Proctor at the United States Department of Agriculture (USDA). This gene is present in the *A. niger* fumonisin biosynthetic gene cluster, however it is not involved in biosynthesis¹⁸. We decided to investigate this gene product since it is an oxidoreductase of unknown function that resides solely within the fumonisin biosynthetic gene cluster of *Aspergilli*, with no homolog in the *Fusarium* spp. cluster. As well, it is a member of the SDR superfamily, many enzymes of which participate in various types of primary and secondary metabolism, usually converting ketone functional groups to hydroxyls⁵⁰. Therefore, if sdr1 is capable of generating FL_a fumonisins, it might explain why FL_a production has only been reported in *Aspergillus* spp., and not in *Fusaria*.

As such, sdr1 was cloned into an N-terminal his-tagged expression vector before attempting purification with nickel immobilized metal affinity chromatography (Ni-IMAC). However, SDS-PAGE analysis showed the protein was poorly expressed and could not be enriched after Ni-IMAC (Figure 9). This construct is predicted to have an approximate molecular weight (MW) of 33.6 kDa, and there is no visible band at this MW in the 300 mM imidazole elution fraction.

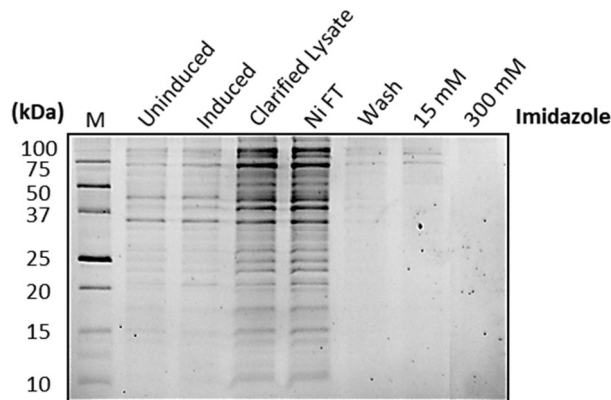


Figure 9. SDS-PAGE of Ni-IMAC purification of *A. niger* sdr1. Each lane represents, from left to right, the protein marker, cell lysate from uninduced *E. coli*, cell lysate from induced *E. coli*, the soluble fraction of cell lysate after high-speed centrifugation, Ni column flowthrough, 10 mM imidazole wash (NiA buffer), 15 mM imidazole wash, and 300 mM imidazole elution (NiB buffer). Numbers on the left correspond to the molecular weight, in kDa, of protein markers used as a standard.

Phyre² analysis indicated that *A. niger* sdr1 likely contains a conserved transmembrane helix at its C-terminus (Figure 10). To improve expression and solubility, a C-terminal truncated version of the protein was generated by incorporating a stop codon after residue R248, eliminating the final 41 residues and putative C-terminal transmembrane helix from the protein, and termed sdr1_CA248. SDS-PAGE analysis showed that expression and solubility remained poor for this construct (Figure 11). There is a faint band (highlighted in red) in the cell lysate following induction in *E. coli* that corresponds to this construct's predicted MW of 29.13 kDa, however it is not present in the clarified lysate or any of the imidazole washes or elutions. As such, sdr1_CA248 was cloned into a his-tagged expression vector containing an N-terminal maltose-binding protein (MBP) tag via Gateway[®] cloning in an effort to increase its solubility. Attempted Ni-IMAC purification of this construct was again unsuccessful, with no visible purified protein in the 300 mM imidazole elution (Figure 12).

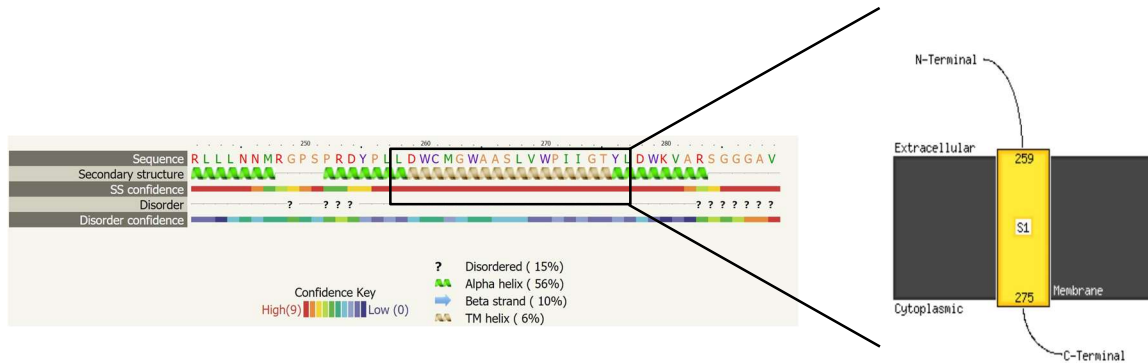


Figure 10. C-terminal secondary structure prediction of *A. niger* sdr1 by Phyre². Structure prediction and disorder confidence are indicated by the colourimetric key from red (high confidence) to indigo (low confidence). sdr1 is predicted to contain a transmembrane helix near its C-terminus with high confidence.

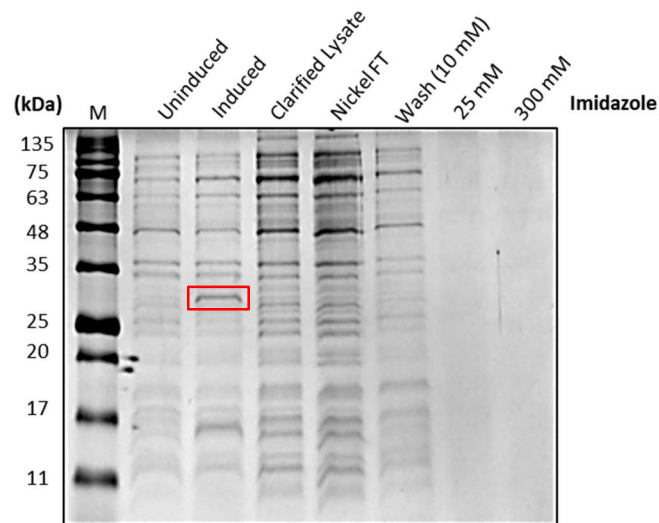


Figure 11. SDS-PAGE of Ni-IMAC purification of *A. niger* sdr1_C Δ 248. Each lane represents, from left to right, the protein marker, cell lysate from uninduced *E. coli*, cell lysate from induced *E. coli*, the soluble fraction of cell lysate after high-speed centrifugation, Ni column flowthrough, 10 mM imidazole wash (NiA buffer), 25 mM imidazole wash, and 300 mM imidazole elution (NiB buffer). Numbers on the left correspond to the molecular weight, in kDa, of protein markers used as a standard.

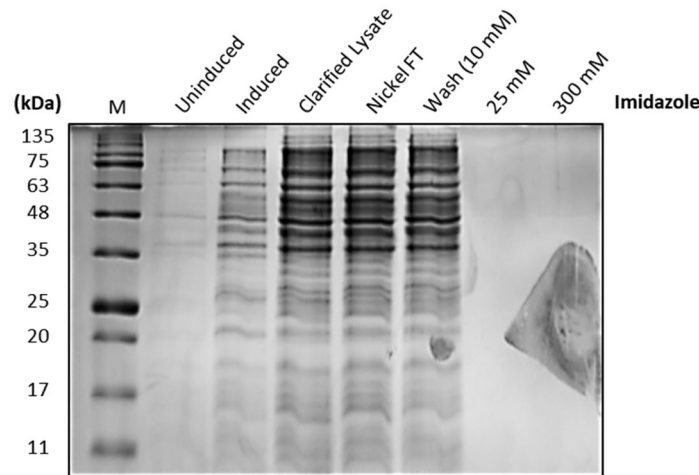


Figure 12. SDS-PAGE of Ni-IMAC purification of MBP-tagged *A. niger* sdr1_C Δ 248. Each lane represents, from left to right, the protein marker, cell lysate from uninduced *E. coli*, cell lysate from induced *E. coli*, the soluble fraction of cell lysate after high-speed centrifugation, Ni column flowthrough, 10 mM imidazole wash (NiA buffer), 25 mM imidazole wash, and 300 mM imidazole elution (NiB buffer). Numbers on the left correspond to the molecular weight, in kDa, of protein markers used as a standard.

This led to further analysis of the sdr1 amino acid sequence to determine potential reasons for its poor expression and solubility. Phyre² also provides secondary structure predictions for proteins most similar to the inputted query, which revealed that our sdr1 construct is likely lacking the third of seven beta-strands that is present in almost all of its closest homologs. Members of the SDR superfamily adopt a highly conserved 3D structure with alternating alpha-helices and beta-strands known as the Rossmann fold⁵⁰. Based on the secondary structure prediction of these close homologs, 3D models provided by Phyre, and structures in the PDB, it is likely that there are also turn segments before and after the beta-strand within the “missing” sequence, as well as the first ~3 residues of the subsequent alpha-helix^{51,52,73}. The missing beta-strand would likely fold into the middle of the underlying beta-sheet, which is sandwiched by three alpha-helices on either side. However, 3D structures also show that residues within this beta-strand likely do not interact with NAD(P)H cofactors⁵¹. Nonetheless, the apparent lack of this

secondary structure unit could explain sdr1's poor expression and solubility, as it is likely required for proper protein folding. Without proper folding, interactions with potential NAD(P)H cofactors and fumonisin substrates would also be hindered.

To address this problem, we investigated some of sdr1's most similar homologs from other strains of *Aspergilli*. A protein BLAST indicated that our sdr1 construct is closely related to a number of other SDR proteins from various strains of *A. niger*, *A. welwitschiae*, and *A. phoenicis* that contain the missing beta-strand. Notably, it appeared most closely related to a protein from *A. phoenicis* (see amino acid sequence analyses below). Since we were interested in sdr1 partially due to its presence in *A. niger*'s fumonisin BGC, we then determined whether this new protein's corresponding gene is located within *A. phoenicis*' fumonisin BGC. A subsequent Clustal Omega multiple sequence alignment of this gene with the entire *A. phoenicis* genome revealed that it is not (data not shown). Because of this, we shifted our focus to the next most closely related protein from the BLAST search, which is from a separate strain of *A. niger* (termed CBS 513.88). After aligning its corresponding gene's sequence with the entire *A. niger* CBS 513.88 genome, we determined it is present in this strain's fumonisin BGC (data not shown).

A Clustal Omega multiple sequence alignment of all three proteins indicated that the *A. phoenicis* SDR was indeed more comparable to our sdr1 construct (99.31 percent identity), however the CBS 513.88 homolog is still very similar with a 97.58 percent identity (Figure 13). Because of its presence in the *A. niger* fumonisin BGC, the CBS 513.88 SDR gene was synthesized by Twist Bioscience in an N-terminal MBP- and

his-tagged expression vector for further analysis and hereon referred to as CBS_sdr1_MBP.

CBS_sdr1	MFVQGNHALVAGGSKGLGREISLALVKRGAVHTVIARSQDALDRKVDMEAVRVHGDQV	60
sdr1	MFVQGNHALVAGGSKGLGREISLALVKRGAVHTVIARSQDALDRKVDME-----	52
A_phoenicis_sdr1	MFVQGNHALVAGGSKGLGREISLALVKRGAVHTVIARSQDALDRKVDMEAVRVHGDQV	60
	*****.*	
CBS_sdr1	IGIQSLDLTNSSEVSRFVQTFGNKITALFCTAGGTDEEVGHFVDIPATSIQSCMEKNYLT	120
sdr1	-----VRFVQTFGNEITALFCTAGGTDEEVGHFVDIPATSIQSCMEKNYLT	99
A_phoenicis_sdr1	IGIQNLDLNSSEVSRFVQTFGNEITALFCTAGGTDEEVGHFVDIPATSIQSCMEKNYLT	120
	******.*	
CBS_sdr1	AAFVAQAVMGTWTELKRVGECGDAQSRHIVFTASTAALVAVPGYAAYSPSKAAIRALA	180
sdr1	AAFVAQAVMRTWTELKRVGECGDAQSRHIVFTASTAALVAVPGYAAYSPSKAAIRALA	159
A_phoenicis_sdr1	AAFVAQAVMRTWTELKRVGECGDAQSRHIVFTASTAALVAVPGYAAYSPSKAAIRALA	180
	*****.*	
CBS_sdr1	DSLRLQESLMYPPAGAIQVHCSFPGTYTDSFYREQARKPQLCKEIEGTVDDGGGLTAKDV	240
sdr1	DSLRLQESLMYPPAGAIQVHCSFPGTYTDSFYREQARKPQLCKEIEGTVDDGGGLTAKDV	219
A_phoenicis_sdr1	DSLRLQESLMYPPAGAIQVHCSFPGTYTDSFYREQARKPQLCKEIEGTVDDGGGLTAKDV	240
	*****.*	
CBS_sdr1	AQRVLVGLDSGCFIPTDLQTRLLNMMRGSPRDYPLDWCWGAASLVWPIIGTYLDW	300
sdr1	AQRVLVGLDSGCFIPTDLQTRLLNMMRGSPRDYPLDWCWGAASLVWPIIGTYLDW	279
A_phoenicis_sdr1	AQRVLVGLDSGCFIPTDLQTRLLNMMRGSPRDYPLDWCWGAASLVWPIIGTYLDW	300
	*****.*	
CBS_sdr1	KVARSGGGTV	310
sdr1	KVARSGGGAV	289
A_phoenicis_sdr1	KVARSGGGAV	310
	*****.*	

Figure 13. Clustal Omega multiple sequence alignment of *A. niger* sdr1 (middle), *A. niger* CBS 513.88 sdr1 (top), and *A. phoenicis* sdr1 (bottom). Asterisks (*) indicate positions with a fully conserved residue, colons (:) indicate conservation between groups of amino acids with strongly similar properties, and periods (.) indicate conservation between groups of amino acids with weakly similar properties. The red squares denote the location of the missing sequence in our sdr1 construct, and its presence in the CBS 513.88 and *A. phoenicis* homologs. The beta-strand of interest is expected to occur from residues 59-65 in these homologs.

After expression in *E. coli*, Ni-IMAC purification of CBS_sdr1_MBP appeared promising: there was a prominent band in the 300 mM imidazole lane at the position corresponding to this construct's predicted MW of 76.32 kDa (Figure 14A). However, analysis by size-exclusion chromatography (SEC) suggested that this construct formed soluble aggregates: most of the injected sample came off the column at its void volume, even though it has a MW cutoff of 600 kDa (Figure 14B-C). Similar to the original sdr1 construct, a Phyre² secondary structure prediction for CBS_sdr1_MBP showed that it likely contains a transmembrane helix at its C-terminus. For this reason,

we incorporated a stop codon after residue R269, eliminating the final 41 residues and predicted helix once again, creating a new construct termed CBS_sdr1_MBP_CΔ269.

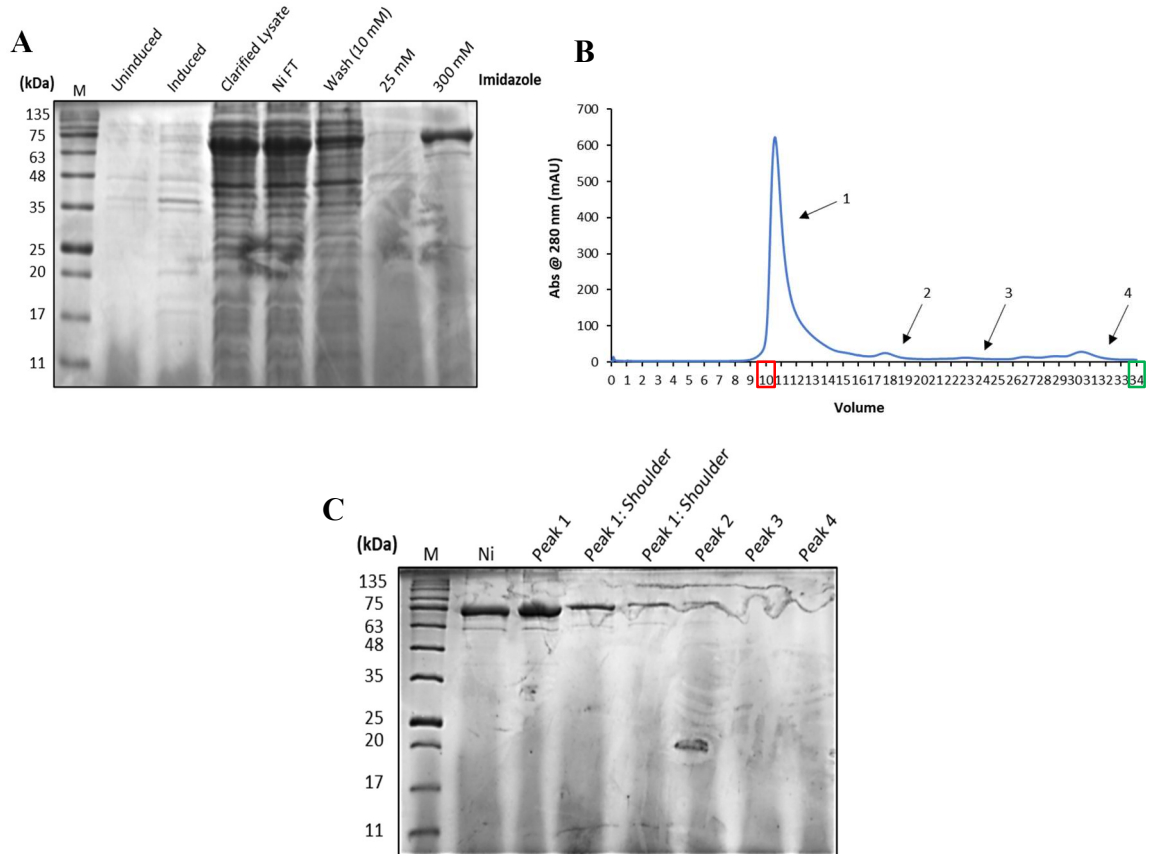


Figure 14. Ni-IMAC and SEC purification of *A. niger* CBS_sdr1_MBP. **A.** SDS-PAGE analysis for Ni-IMAC purification. Each lane represents, from left to right, the protein marker, cell lysate from uninduced *E. coli*, cell lysate from induced *E. coli*, the soluble fraction of cell lysate after high-speed centrifugation, Ni column flowthrough, 10 mM imidazole wash (NiA buffer), 25 mM imidazole wash, and 300 mM imidazole elution (NiB buffer). **B.** SEC chromatogram for CBS_sdr1_MBP. The blue line represents absorbance at 280 nm. Individual peaks analyzed via SDS-PAGE are numbered. Void volume is highlighted in red, total column volume is highlighted in green. **C.** SDS-PAGE analysis for SEC purification. The first two lanes represent the protein marker and the sample from the 300 mM Ni elution injected onto the size-exclusion column, respectively. The remaining lanes represent fractions from each peak denoted in **B**. Numbers on the left in panels **A**, and **C**, correspond to the molecular weight, in kDa, of protein markers used as a standard.

After expression, purification of CBS_sdr1_MBP_CΔ269 (71.85 kDa) was attempted following the same protocol, but similar results were achieved (Figure 15). The

protein again came off the size-exclusion column at its void volume, suggesting the formation of soluble aggregates.

Since the MBP solubility tag may have been responsible for soluble aggregate formation, the CA269-truncated construct was cloned into an alternative expression vector containing an N-terminal glutathione S-transferase (GST) solubility tag via ligation independent cloning (LIC). Figure 16 shows the SDS-PAGE analysis after attempted Ni-IMAC purification of this new CBS_sdr1_GST_CA269 construct. An additional wash at 75 mM imidazole was performed to remove impurities visualized after a previous purification attempt (data not shown), however, most of the protein eluted from the column during this wash. As a result, this fraction was dialyzed to remove imidazole and lower the NaCl concentration before assaying for FLa-generating activity.

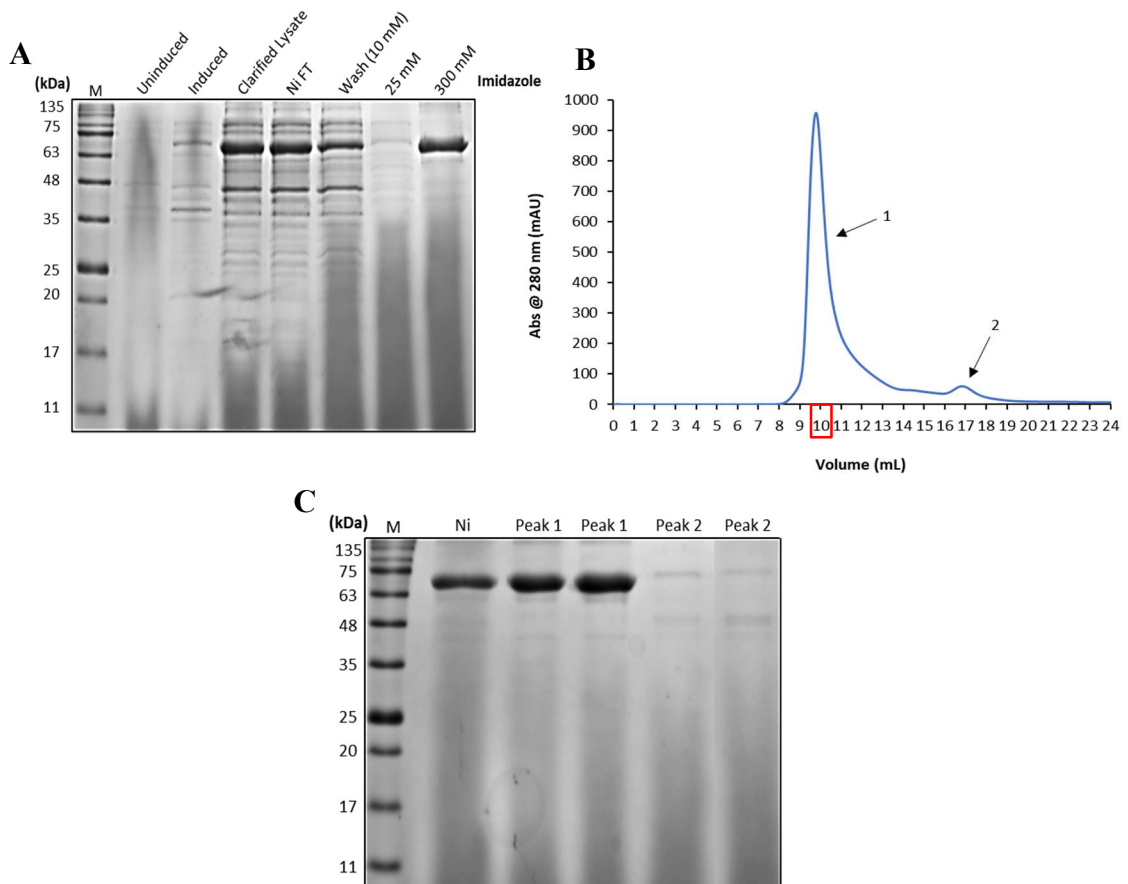


Figure 15. Ni-IMAC and SEC purification of *A. niger* CBS_sdr1_MBP_CΔ269. **A.** SDS-PAGE analysis for Ni-IMAC purification. Each lane represents, from left to right, the protein marker, cell lysate from uninduced *E. coli*, cell lysate from induced *E. coli*, the soluble fraction of cell lysate after high-speed centrifugation, Ni column flowthrough, 10 mM imidazole wash (NiA buffer), 25 mM imidazole wash, and 300 mM imidazole elution (NiB buffer). **B.** SEC chromatogram for CBS_sdr1_MBP_CΔ269. The blue line represents absorbance at 280 nm. Individual peaks analyzed via SDS-PAGE are numbered. Void volume is highlighted in red. Total column volume occurred at 34 mL on the x-axis; the chromatogram was condensed for clarity. **C.** SDS-PAGE analysis for SEC purification. The first two lanes represent the protein marker and the sample from the 300 mM Ni elution injected onto the size-exclusion column, respectively. The remaining lanes represent fractions from each peak denoted in **B.** Numbers on the left in panels **A.** and **C.** correspond to the molecular weight, in kDa, of protein markers used as a standard.

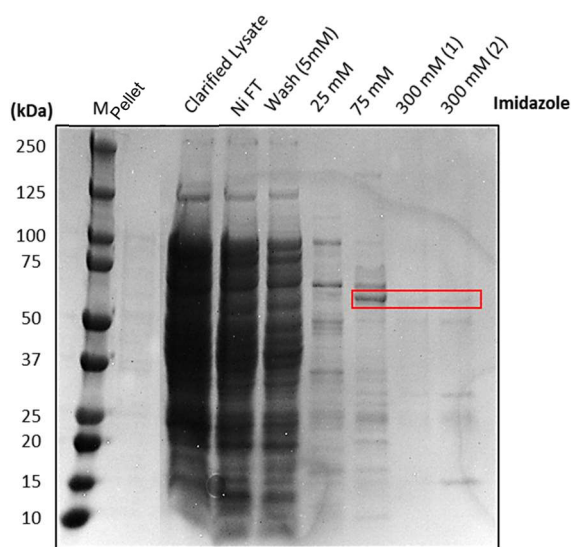


Figure 16. SDS-PAGE of Ni-IMAC purification of CBS_sdr1_GST_CΔ269. Each lane represents, from left to right, the protein marker, the cell lysate pellet after high-speed centrifugation, the soluble fraction of cell lysate after high-speed centrifugation, Ni column flowthrough, 5 mM imidazole wash (NiA buffer), 25 mM imidazole wash, 75 mM imidazole elution, and 300 mM imidazole elution (NiB buffer) x2 (each lane represents one CV). Numbers on the left correspond to the molecular weight, in kDa, of protein markers used as a standard.

Two of the above constructs with the most promising purification results were tested for FLa-generating activity: *A. niger* CBS_sdr1_MBP_CΔ269 and *A. niger* CBS_sdr1_GST_CΔ269. For the MBP-tagged construct, fractions from both SEC peaks in Figure 15 were tested, with ~25 μM enzyme used for peak 1, and ~2 μM enzyme for

peak 2. For the GST-tagged construct, the dialyzed 75 mM imidazole fraction from Figure 16 was concentrated to ~15 μ M for the LC-MS assay. Each enzyme was incubated with ~7 μ M FB₁, FB₂, FPy₁, and FPy₂ separately overnight at room temperature and 37°C. 10 μ M of both NADH and NADPH were also included as potential cofactors, since we hypothesized that *sdr1* was a member of the NAD(P)H-dependent SDR superfamily. Unfortunately, no FLa fumonisins were observed by mass spectrometry in any of the reaction conditions (data not shown). These results, combined with poor protein solubility and aggregation for all *sdr1* constructs, led us to focus on FUM13 as a potential FLa-generating enzyme instead.

3.3.2 A. niger FUM13

FUM13 is present in both the *Aspergillus* and *Fusarium* fumonisin biosynthetic gene clusters and is also a member of the SDR superfamily (Figure 17A). This enzyme plays a key role in fumonisin biosynthesis, reducing the C-3 carbonyl group on a 3-keto FB intermediate to a hydroxyl (Figure 17B)⁴⁹. This intermediate is structurally similar to FPy fumonisins; the carbonyl is located only one carbon length away relative to its C-2 position in FPy. The biggest differences in their structures are the lack of TCE sidechains and the presence of a C-2 amine in the 3-keto FB intermediate. Overall, FUM13's presence in these species' fumonisin biosynthetic gene clusters, and the similarity between its native substrate and FPy fumonisins, led us to hypothesize that it may be capable of catalyzing FPy to FLa reduction.

As such, the *A. niger* FUM13 gene was synthesized and expressed as an N-terminal his-tagged construct in a similar fashion to the *sdr1* gene and its homolog. After

sonication, the cell lysate was clarified by centrifugation and loaded onto a nickel column for purification by IMAC. A low yield of FUM13 was eluted from the nickel column with 300 mM imidazole (~1 mg of protein from a 2 L bacterial expression), however the protein was relatively pure according to SDS-PAGE analysis (Figure 18). This fraction was dialyzed overnight at 4°C to remove imidazole and lower the NaCl concentration before concentrating the protein and assaying for FLa-generating activity.

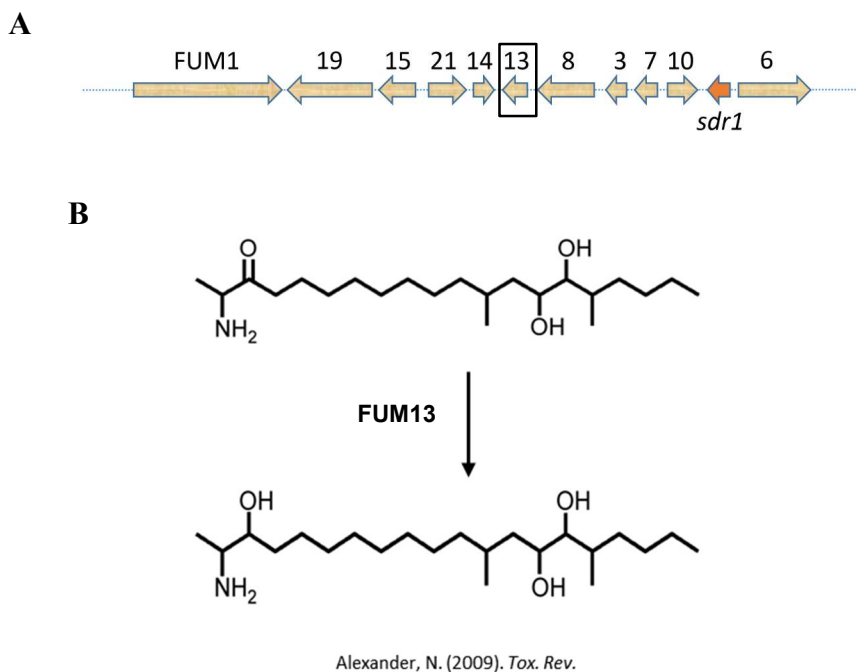


Figure 17. Native mechanism of FUM13 in fumonisin biosynthesis. **A.** Schematic of the *A. niger* fumonisin biosynthetic gene cluster with FUM13 highlighted. **B.** FUM13 naturally catalyzes the 4th step in fumonisin biosynthesis: reduction of the ketone on 3-keto FB fumonisin biosynthetic intermediates to a hydroxyl to create a 3-hydroxy FB intermediates.

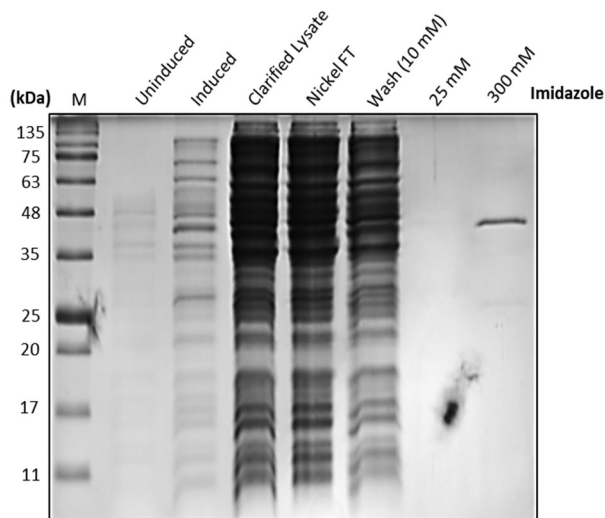


Figure 18. SDS-PAGE of Ni-IMAC purification of *A. niger* FUM13. Each lane represents, from left to right, the protein marker, cell lysate from uninduced *E. coli*, cell lysate from induced *E. coli*, the soluble fraction of cell lysate after high-speed centrifugation, Ni column flowthrough, 10 mM imidazole wash (NiA buffer), 25 mM imidazole wash, and 300 mM imidazole elution (NiB buffer). Numbers on the left correspond to the molecular weight, in kDa, of protein markers used as a standard.

Similar reactions to the *sdr1* constructs were performed for this enzyme: ~10 μM *A. niger* FUM13 was incubated with ~3.5 μM FB₁, FB₂, FPy₁, and FPy₂ separately at room temperature and 37°C for a period of 4 days. 50 μM NADPH was included as a potential cofactor for these and all other FUM13 reactions, as Yi *et al.* used this cofactor and concentration when elucidating the enzyme's native function in *F. verticillioides*⁴⁹. After incubation with FB₁ and FB₂, no FL_a fumonisins were observed by mass spectrometry for either temperature (data not shown). In comparison, both FL_{a1} and FL_{a2} were generated after incubation with FPy₁ and FPy₂, respectively (Figure 19). Room temperature reactions were more efficient than at 37°C, and FPy₂ appeared to be the best substrate as FL_{a2} was produced in much greater amounts than FL_{a1}. However, the enzyme was very inefficient; the maximum percent conversion for any of the conditions was less than 2.5% (room temperature, FPy₂ substrate). Nonetheless, this was the first

time reliable FL_a signals had been observed by mass spectrometry after incubating fumonisin substrates with a recombinant enzyme. This data also suggests that FUM13 is indeed using FPy fumonisins as substrates for FL_a generation, as opposed to FB forms or a separate mechanism entirely.

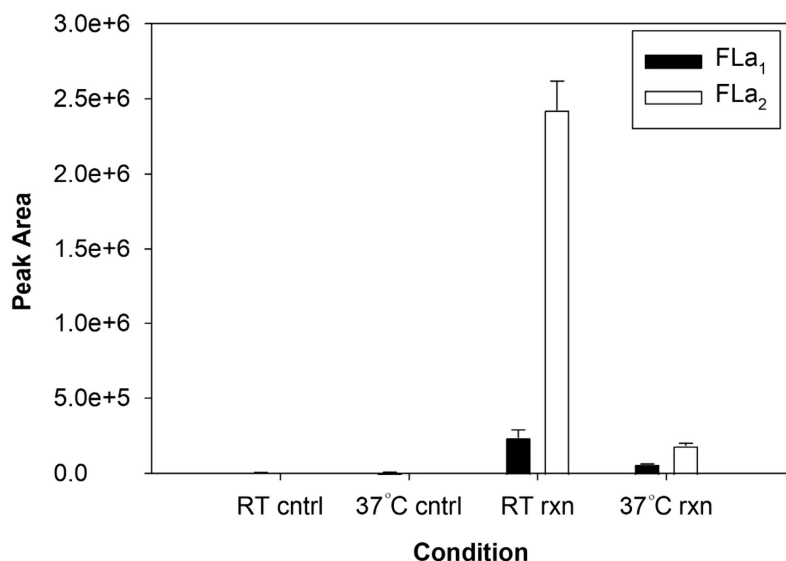


Figure 19. *A. niger* FUM13 partially reduces FPy₁ and FPy₂ over 4 days. The enzyme was purified via nickel affinity chromatography and dialyzed overnight to reduce salt and imidazole concentrations. FL_a amounts for each condition are illustrated by LC-MS peak area. Peak areas are the means \pm SEM of 3 *in vitro* replicates. FL_{a1} and FL_{a2} levels are shown for each control and reaction condition.

Because of the low yields obtained after Ni-IMAC (~1 mg of protein from a 2 L bacterial expression), and the inefficient reduction of FPy fumonisins to FL_a forms, LIC was used to insert *A. niger* FUM13 into a new expression vector containing an N-terminal GST tag to increase protein solubility. This new construct (termed *A. niger* FUM13_GST) was expressed in a similar manner to untagged FUM13 before partial purification by Ni-IMAC. Figure 20 shows the SDS-PAGE analysis before dialysis and assaying for FL_a-generating activity. Overall, this shows that the GST tag increased FUM13 solubility considerably: the most prominent band in the 300 mM imidazole lane

corresponds to this construct's MW of ~67 kDa. Protein yields also increased to ~5.5 mg per 2 L of bacterial expression.

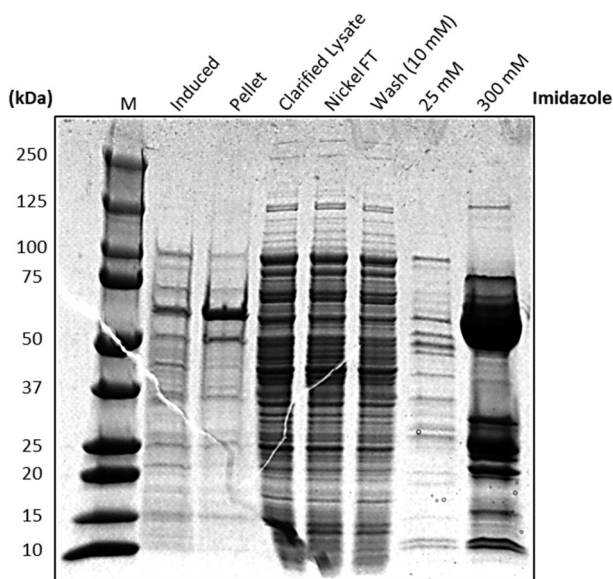


Figure 20. SDS-PAGE of Ni-IMAC purification of *A. niger* FUM13_GST. Each lane represents, from left to right, the protein marker, cell lysate from induced *E. coli*, cell lysate pellet after high-speed centrifugation, the soluble fraction of cell lysate after high-speed centrifugation, Ni column flowthrough, 10 mM imidazole wash (NiA buffer), 25 mM imidazole wash, and 300 mM imidazole elution (NiB buffer). Numbers on the left correspond to the molecular weight, in kDa, of protein markers used as a standard.

The 300 mM imidazole fraction was then dialyzed to remove imidazole and lower NaCl concentration, before concentrating the protein for the following LC-MS assays. In a similar manner to the untagged *A. niger* FUM13 reactions, the protein was incubated with FB₁, FB₂, FPy₁, and FPy₂ separately at room temperature and 37°C, again using 50 μM NADPH as a cofactor. For this construct, separate reactions were performed overnight and for a 4 day period. However, no FLa fumonisins were observed by mass spectrometry under any of the reaction conditions (data not shown). This suggested that the GST tag may be interfering with catalysis, or that this construct may also be forming soluble aggregates, which could be confirmed by future size-exclusion analysis.

3.3.3 *F. verticillioides* FUM13

Since the untagged *A. niger* FUM13 construct showed promising yet inefficient FLa-generating activity, we decided to test its homolog from *F. verticillioides* in an effort to observe more efficient FPy reduction. While neither FPy nor FLa production by *Fusarium* spp. has been reported in the literature, we hypothesized that *F. verticillioides* FUM13 may be capable of reducing FPy fumonisins to their FLa forms. Once again, this gene was synthesized by Twist Bioscience, this time in an N-terminal MBP- and his-tagged expression vector (termed *F. verticillioides* FUM13_MBP). It was expressed in a similar manner to all previous constructs before lysis and clarification by centrifugation. *F. verticillioides* FUM13_MBP was then partially purified from the cell lysate by Ni-IMAC (Figure 21A). SDS-PAGE analysis showed very promising results after the nickel column; *F. verticillioides* FUM13_MBP appeared sufficiently soluble for purification and is clearly the predominant protein eluted in the 300 mM imidazole condition.

The partially purified sample from Ni-IMAC was loaded onto a size-exclusion column equilibrated with 50 mM Tris, pH 8.0, and 50 mM NaCl. Panels B and C in Figure 21 show the chromatogram and SDS-PAGE analysis of the SEC purification. Peak 1 is likely due to the formation of soluble aggregates of *F. verticillioides* FUM13_MBP. It appears later than the void volume (650 kDa MW cutoff), yet significantly earlier than what would be expected for this 83.44 kDa protein. Additionally, no FLa fumonisins were produced when this fraction was incubated with FPy substrates, in contrast to fractions from the second peak.

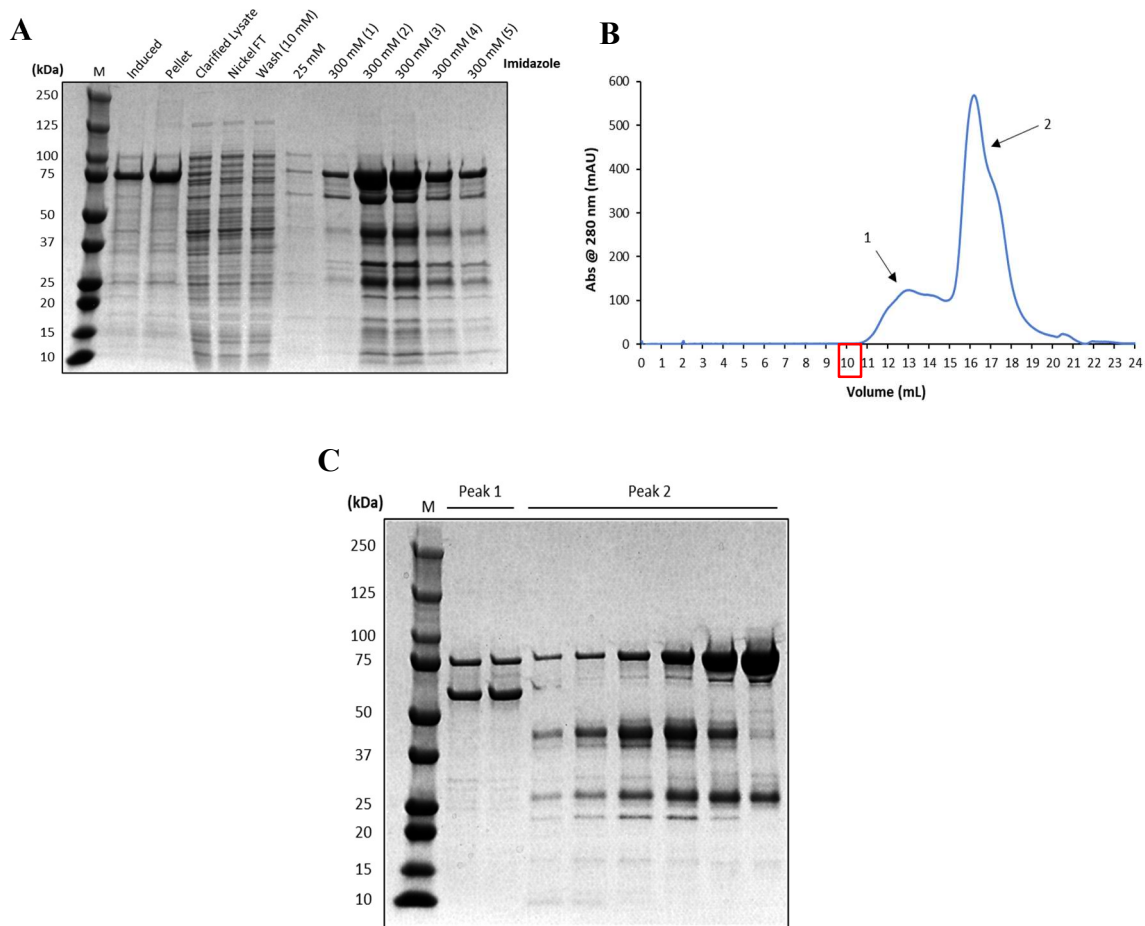


Figure 21. Ni-IMAC and SEC purification of *F. verticillioides* FUM13_MBP. **A.** SDS-PAGE analysis for Ni-IMAC purification. Each lane represents, from left to right, the protein marker, cell lysate from induced *E. coli*, cell lysate pellet after high-speed centrifugation, the soluble fraction of cell lysate after high-speed centrifugation, Ni column flowthrough, 10 mM imidazole wash (NiA buffer), 25 mM imidazole wash, and 300 mM imidazole elution (NiB buffer) x5 (each lane represents one CV). **B.** SEC chromatogram for *F. verticillioides* FUM13_MBP. The blue line represents absorbance at 280 nm. Individual peaks analyzed via SDS-PAGE are numbered. Void volume is highlighted in red. Total column volume occurred at 34 mL on the x-axis; the chromatogram was condensed for clarity. **C.** SDS-PAGE analysis for SEC purification. The first lane represents the protein marker, the remaining lanes represent fractions from each peak denoted in **B.** Numbers on the left in panels **A.** and **C.** correspond to the molecular weight, in kDa, of protein markers used as a standard.

Importantly, since our protoplast and *A. niger* FUM13 assays were only successful when using FPy forms as substrates, no FB fumonisins were used for the following *F. verticillioides* FUM13 experiments. As well, reactions were only performed

at 37°C since previous assays with this protein showed less efficient conversion at room temperature (data not shown).

The first FUM13 assay was conducted with protein samples from peak 2 in Figure 21. ~16.5 μM *F. verticillioides* FUM13_MBP was incubated separately with ~110 μM FPy₁, ~110 μM FPy₂, and ~0.6 μM ¹³C-FPy₂ overnight at 37°C. We used ¹³C-FPy₂ in addition to the unlabeled congeners as a pseudo-control to ensure that the low levels of FL_a fumonisins we were observing on the mass spectrometer were not errant background signals. Figure 22 shows the percent conversion of FPy fumonisins to FL_a forms after the overnight reaction with each of the three FPy substrates. Comparing FPy₁ and FPy₂, the latter appeared the preferred substrate, as was the case with *A. niger* FUM13. After the FPy₂ reaction, ~30% of the fumonisins present were FL_{a2}, as opposed to ~20% FL_{a1} for the FPy₁ reaction. Notably, the reaction appeared much more efficient when using ¹³C-FPy₂ as a substrate, likely because its concentration in the reaction was much lower than FPy₁ and FPy₂ (¹³C-labeled fumonisins are commercially available in much lower concentrations than their unlabeled congeners). After this reaction, more than 80% of the fumonisins present were ¹³C-FL_{a2}; the highest enzymatic conversion efficiency observed thus far.

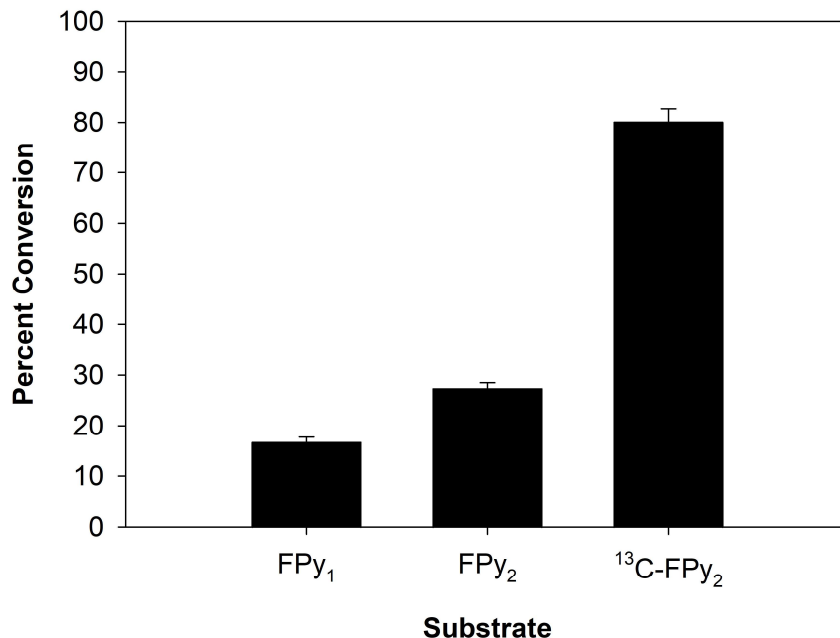


Figure 22. *F. verticillioides* FUM13_MBP partially reduces FPy₁, FPy₂, and ¹³C-FPy₂ overnight. The enzyme was purified via nickel affinity chromatography followed by size-exclusion chromatography and buffer exchange to reduce salt concentration and remove imidazole. Fumonisin amounts are illustrated by the percent conversion of FPy substrates to FLa forms. Percentages are the means ± SEM of 3 *in vitro* replicates.

Given the greater efficiency when using ¹³C-FPy₂ as a substrate, we wanted to repeat these reactions with FPy₁ and FPy₂ at the same lower concentration to observe more efficient reduction to their FLa forms. As such, we purified the protein again by Ni-IMAC and SEC (Figure 23). We achieved similar results to the first purification, however there was an additional peak on the SEC chromatogram (Figure 23B). Because of this, protein samples from multiple fractions of the SEC purification in Figure 23 were used for this assay. The fractions used, and the portion of the chromatogram they correspond to, are as follows: F4 (peak 1), F11 (peak 2), F12 (valley between peaks 2 and 3), F13 (peak 3), and F14 (shoulder of peak 3). The protein concentration for each fraction used in the assay was ~13 μM, and the FPy concentration in each reaction was ~0.6 μM. Reactions were performed overnight at 37°C, again with 50 μM NADPH included as a

cofactor. For the F4 reaction, which most likely contained soluble protein aggregates, no FL_a fumonisins were observed after incubation with either substrate (data not shown). Figure 24 shows the percent conversion of FP_y fumonisins to FL_a forms after the overnight reaction with each of F11-F14. All four of these fractions appeared similarly active, with a slight decline in reaction efficiency from F11 to F14. Once again, FP_{y2} appeared to be the preferred substrate, with near 100% reduction to FL_{a2} for F11 and F12, and greater than 90% for F13 and F14. Reduction of FP_{y1} to FL_{a1} was less efficient, however this was still the greatest reduction efficiency for the 1 series fumonisins that we have observed. After the overnight reactions using F11 and F12, FL_{a1} constituted between 70-80% of the fumonisins present, whereas for F13 and F14, FL_{a1} constituted only ~55% and ~45%, respectively.

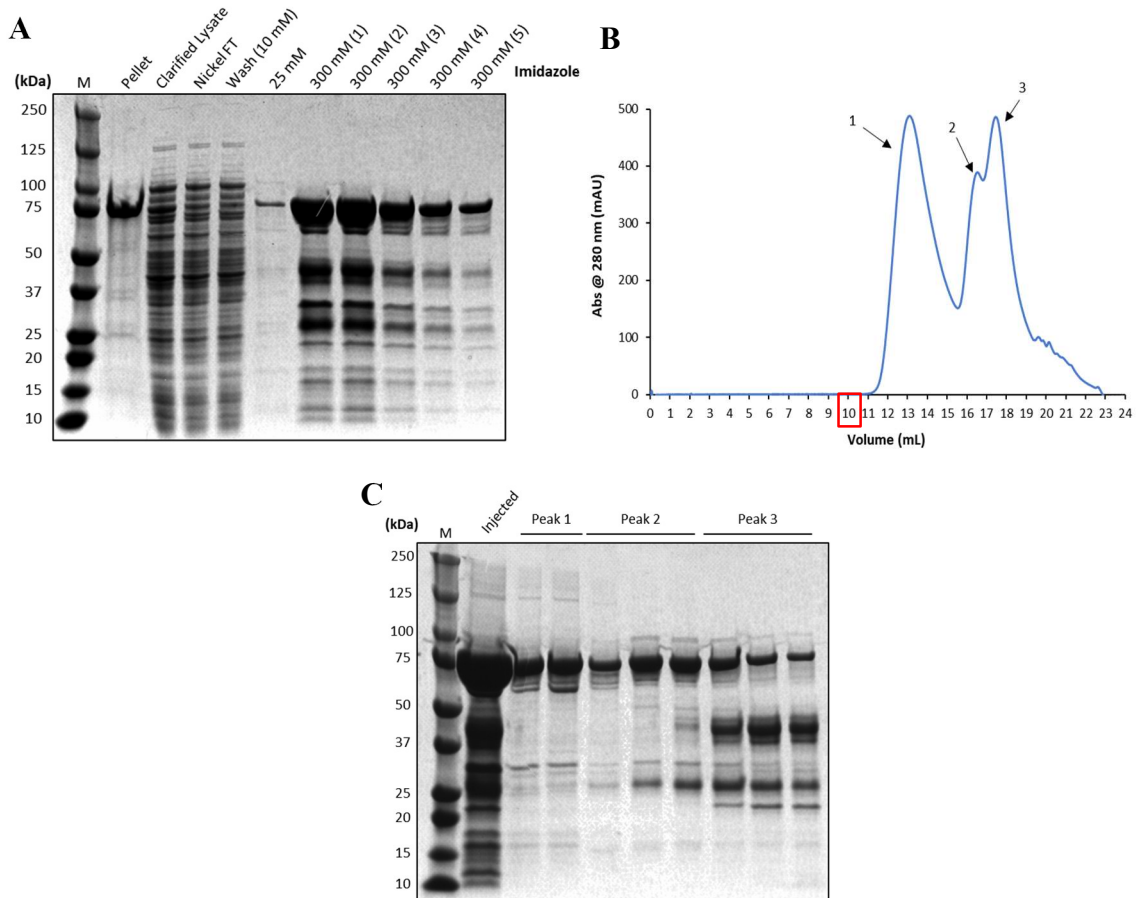


Figure 23. Ni-IMAC and SEC purification of *F. verticillioides* FUM13_MBP. **A.** SDS-PAGE analysis for Ni-IMAC purification. Each lane represents, from left to right, the protein marker, cell lysate pellet after high-speed centrifugation, the soluble fraction of cell lysate after high-speed centrifugation, Ni column flowthrough, 10 mM imidazole wash (NiA buffer), 25 mM imidazole wash, and 300 mM imidazole elution (NiB buffer) x5 (each lane represents one CV). **B.** SEC chromatogram for *F. verticillioides* FUM13_MBP. The blue line represents absorbance at 280 nm. Individual peaks analyzed via SDS-PAGE are numbered. Void volume is highlighted in red. Total column volume occurred at 34 mL on the x-axis; the chromatogram was condensed for clarity. **C.** SDS-PAGE analysis for SEC purification. The first two lanes represent the protein marker and the sample from the 300 mM Ni elution injected onto the size-exclusion column (after concentration), respectively. The remaining lanes represent fractions from each peak denoted in **B.** Numbers on the left in panels **A.** and **C.** correspond to the molecular weight, in kDa, of protein markers used as a standard.

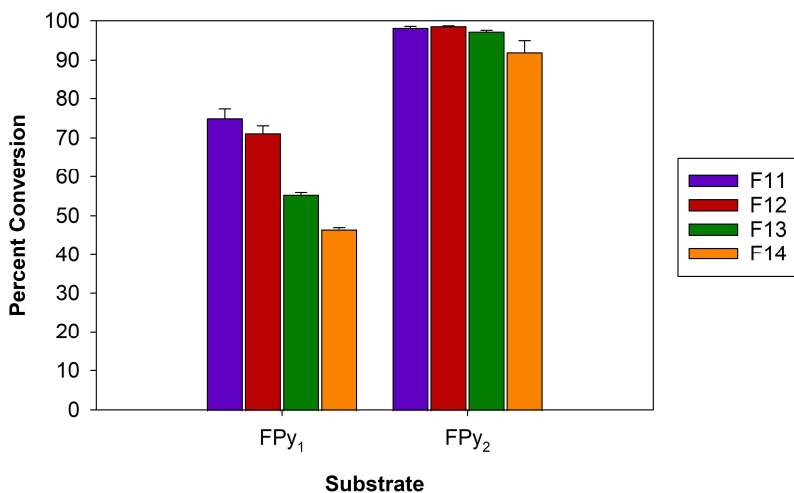


Figure 24. *F. verticillioides* FUM13_MBP reduces FPy₁ and FPy₂ overnight. The enzyme was purified via nickel affinity chromatography followed by size-exclusion chromatography and buffer exchange to reduce salt concentration and remove imidazole. Fumonisin amounts are illustrated by the percent conversion of FPy substrates to FLa forms. Percentages are the means \pm SEM of 3 *in vitro* replicates.

Given this success with *F. verticillioides* FUM13_MBP, we next tested how effective the enzyme would be at lower concentrations in the presence of higher substrate concentrations. We tested the enzyme at 1 μ M and 100 nM with increasing concentrations of FPy₁ and FPy₂ (5.6 μ M, 28 μ M, and 56 μ M).

Regardless of substrate concentration, 100 nM *F. verticillioides*

FUM13_MBP was unable to reduce FPy₁ or FPy₂ (data not shown). However, at 1 μM the enzyme reduced both FPy₁ and FPy₂ to their FLa forms, although reaction efficiencies were very low once again: the ~10% conversion of 5.6 μM FPy₂ to FLa₂ was the most efficient reaction (Figure 25). For both substrates, conversion was more efficient at decreasing FPy concentrations. FPy₂ again appeared to be the preferred substrate compared to FPy₁. In fact, a higher conversion rate was observed for the least efficient FPy₂ reaction (56 μM substrate) than for the most efficient FPy₁ reaction (5.6 μM substrate); both ~4%.

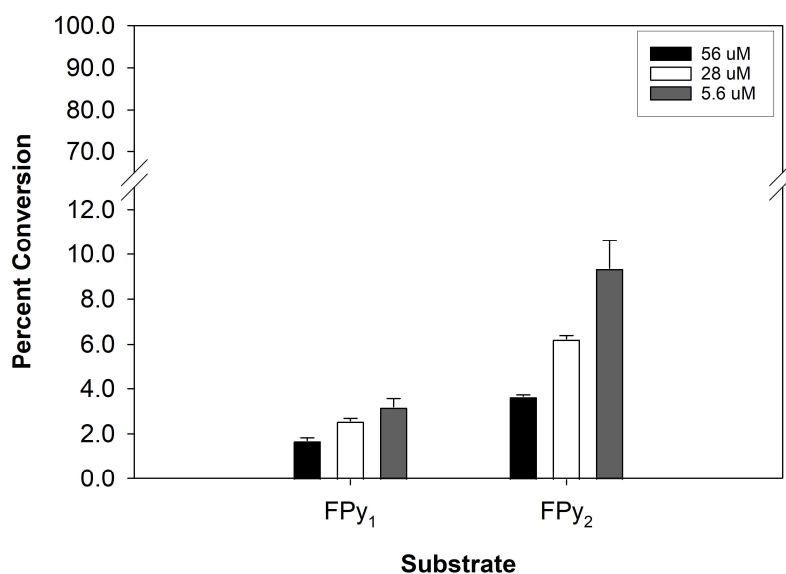


Figure 25. 1 μM *F. verticillioides* FUM13_MBP partially reduces increased amounts of FPy₁ and FPy₂ overnight. The enzyme was purified via nickel affinity chromatography followed by size-exclusion chromatography and buffer exchange to reduce salt concentration and remove imidazole. Fumonisin amounts are illustrated by the percent conversion of FPy substrates to FLa forms. Percentages are the means ± SEM of 3 *in vitro* replicates.

3.4 Discovery of an FPy-Generating *F. verticillioides* Amine Oxidase

Our data indicated that *F. verticillioides* FUM13 is capable of inefficiently generating FLA fumonisins *in vitro*. This led other members of the Garnham and Sumarah labs to monitor the production of FPy and FLA fumonisins by strains of *F. verticillioides* grown in liquid culture.

Megan Kelman, a technician in the Sumarah lab, grew *F. verticillioides* and monitored for fumonisin production by LC-MS. She indeed detected the presence of FPy and FLA fumonisins within certain strains (Figure 26). While both FB₁ and FB₂ levels were much higher than their FPy and FLA counterparts, this is the first indication of FPy and FLA production by *F. verticillioides*. FLA₂ was the most abundant of the post-biosynthetically modified fumonisins, followed by FPy₁, FPy₂, then FLA₁.

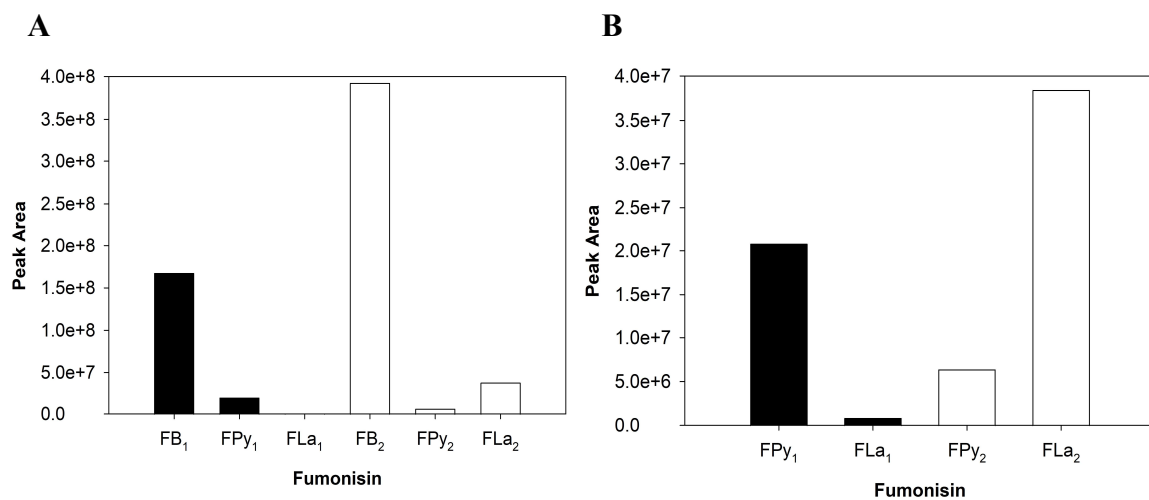


Figure 26. Abundance of the 1 and 2 series fumonisins in *F. verticillioides* culture supernatant from the highest FPy- and FLA-producing strain. The fungus was inoculated in modified MYRO media and grown for a period of 6 weeks. Fumonisin amounts from each strain are illustrated by LC-MS peak area. **A.** Relative levels for FB₁, FPy₁, FLA₁, FB₂, FPy₂, and FLA₂ fumonisins. **B.** Relative levels for the post-

biosynthetically modified fumonisins; FPy₁, FL_{a1}, FPy₂, and FL_{a2}. Note: FB₁ and FPy₁ peak areas also include the less abundant *iso*-FB₁ and *iso*-FPy₁ congeners.

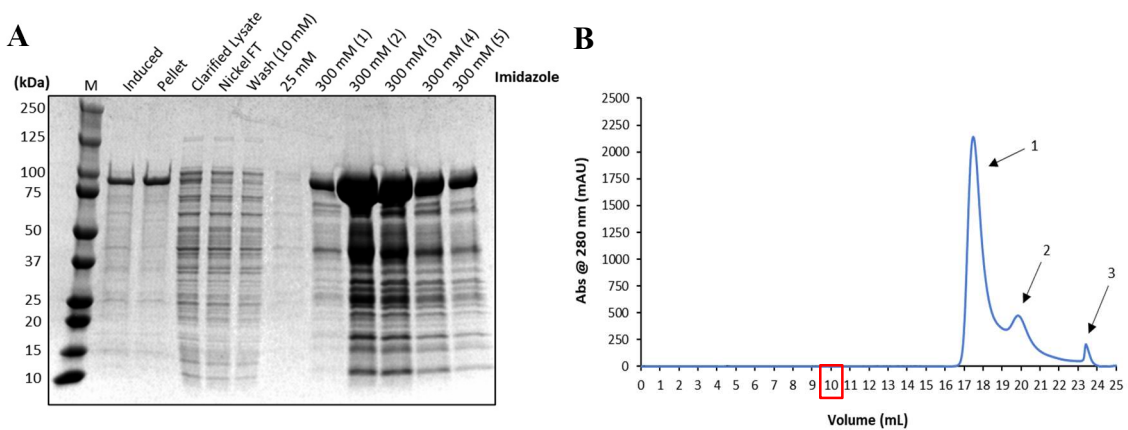
The presence of FPy fumonisins in *F. verticillioides* liquid culture indicated that an enzyme similar to AnFAO is likely responsible for their production. The most closely related homolog to AnFAO in *F. verticillioides* was identified from GenBank-NCBI strain 7600 (a known fumonisin producer) and termed FvFAO (*Fusarium verticillioides* **F**umonisin **A**mine **O**xidase). However, even though FvFAO is AnFAO's most similar homolog in this species, a Clustal Omega multiple sequence alignment showed that they share a percent identity of 44.71 (Figure 27). This gene was synthesized by Twist Bioscience in an N-terminal MBP- and his-tagged expression vector. Dr. Patrick Telmer and Angelo Kaldis initially purified the protein before assaying for FB to FPy deamination activity by LC-MS.



Figure 27. Clustal Omega multiple sequence alignment of AnFAO (top) and FvFAO (bottom). Asterisks (*) indicate positions with a fully conserved residue, colons (:) indicate conservation between groups of amino acids with strongly similar properties, and periods (.) indicate conservation between groups of amino acids with weakly similar properties.

Since AnFAO deaminates sphinganine more efficiently than fumonisins⁴⁸, they also tested FvFAO's activity towards sphinganine. After purifying the enzyme by Ni-IMAC and SEC, it was incubated separately with 1 μ M FB₁, FB₂, and sphinganine overnight at 37°C. Overall, their work showed that FvFAO fully deaminated each substrate overnight (data not shown).

Given these promising results, we decided to purify the protein again and compare its activity to AnFAO using a colourimetric Amplex Red assay, before also determining its kinetic parameters for FB₁ and sphinganine substrates (data shown in section 3.5). After expression, the protein was first purified by Ni-IMAC (Figure 28A) before concentrating and loading onto a size-exclusion column equilibrated with 50 mM MES, pH 6.0, and 100 mM NaCl. Figure 28B & C show the chromatogram and SDS-PAGE analysis of the SEC run. The majority of the protein eluted in the first peak, as expected based on the previous purification trial and the construct's predicted MW of 51.5 kDa. As such, the second fraction of peak 1 was used for the AmplexTM Red assays to follow.



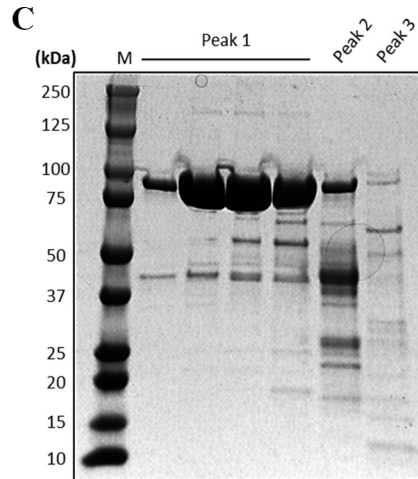


Figure 28. Ni-IMAC and SEC purification of MBP-tagged *F. verticillioides* AnFAO homolog FvFAO. **A.** SDS-PAGE analysis for Ni-IMAC purification. Each lane represents, from left to right, the protein marker, cell lysate from induced *E. coli*, cell lysate pellet after high-speed centrifugation, the soluble fraction of cell lysate after high-speed centrifugation, Ni column flowthrough, 10 mM imidazole wash (NiA2 buffer), 25 mM imidazole wash, and 300 mM imidazole elution (NiB2 buffer) x5 (each lane represents one CV). **B.** SEC chromatogram for FvFAO. The blue line represents absorbance at 280 nm. Individual peaks analyzed via SDS-PAGE are numbered. Void volume is highlighted in red. Total column volume occurred at 34 mL on the x-axis; the chromatogram was condensed for clarity. **C.** SDS-PAGE analysis for SEC purification. The first lane represents the protein marker, the remaining lanes represent fractions from each peak denoted in **B.** Numbers on the left in panels **A.** and **C.** correspond to the molecular weight, in kDa, of protein markers used as a standard.

3.5 Biochemical Characterization of *F. verticillioides* Amine Oxidase FvFAO

All MAOs, including FvFAO and AnFAO, belong to the flavin-dependent amine oxidase superfamily and use Flavin Adenine Dinucleotide (FAD) as a cofactor during catalysis⁵³⁻⁵⁵. Assuming FvFAO follows the same mechanism as AnFAO, it catalyzes the deamination of FB fumonisins to FPy forms via an imine intermediate⁴⁸. During this reaction step, FAD is reduced before being reoxidized by molecular oxygen, producing H₂O₂ as a by-product. The Amplex™ Red assay takes advantage of H₂O₂ production using horseradish peroxidase (HRP). HRP uses H₂O₂ to catalyze the

conversion of AmplexTM Red to resorufin, which absorbs at 571 nm. Crucially, H₂O₂ reacts in a 1:1 manner with AmplexTM Red to produce an equal ratio of resorufin, and monitoring the linear increase in absorbance at 571 nm allows for initial rate calculations. We also incubated increasing concentrations of H₂O₂ with AmplexTM Red and HRP to generate a standard curve to convert absorbance data from units of absorbance/time to enzyme activity in units of molarity/time (Figure 30D). To begin, we utilized this plate-based assay to monitor the activity of FvFAO relative to AnFAO.

3.5.1 Relative Rates for FvFAO vs. AnFAO

Each of the MBP-tagged enzymes were purified by Ni-IMAC and SEC before performing relative rate assays with FB₁, FB₂, and sphinganine substrates. Enzyme and substrate concentrations were held constant, with 50 nM enzyme and 100 μM substrate used for the FB₁ and FB₂ reactions, and 20 nM enzyme with 50 μM substrate used for the sphinganine reactions. The results of each assay, and subsequent relative & absolute rates, are shown in Figure 29 and Table 1, respectively. For both FB₁ and FB₂, FvFAO was approximately 5-fold less active than AnFAO (Figure 29A & B), however for sphinganine it was slightly closer, exhibiting ~30% the activity (Figure 29C). Figure 29D shows the raw absorbance data for the three AnFAO/FB₂ replicates as an illustration; similar outputs were used for each enzyme/substrate combination to calculate initial rates.

Table 1 shows the absolute rates for each condition, where FvFAO's substrate preference and significantly lower activity compared to AnFAO is very clear. Notably, FvFAO was over 5 times as active towards FB₂ relative to FB₁, even though *F. verticillioides* generally produces more FB₁ fumonisins than FB₂. Moreover, AnFAO's

activity towards FB₁ is almost exactly equivalent to FvFAO's towards FB₂. The initial reaction rate for FvFAO towards FB₁ is extremely low at 2.53 nM/min, just above the lower limit for reliable readings from this assay. However, even with its significantly lower activity, we also characterized FvFAO's kinetic parameters for FB₁ and sphinganine substrates.

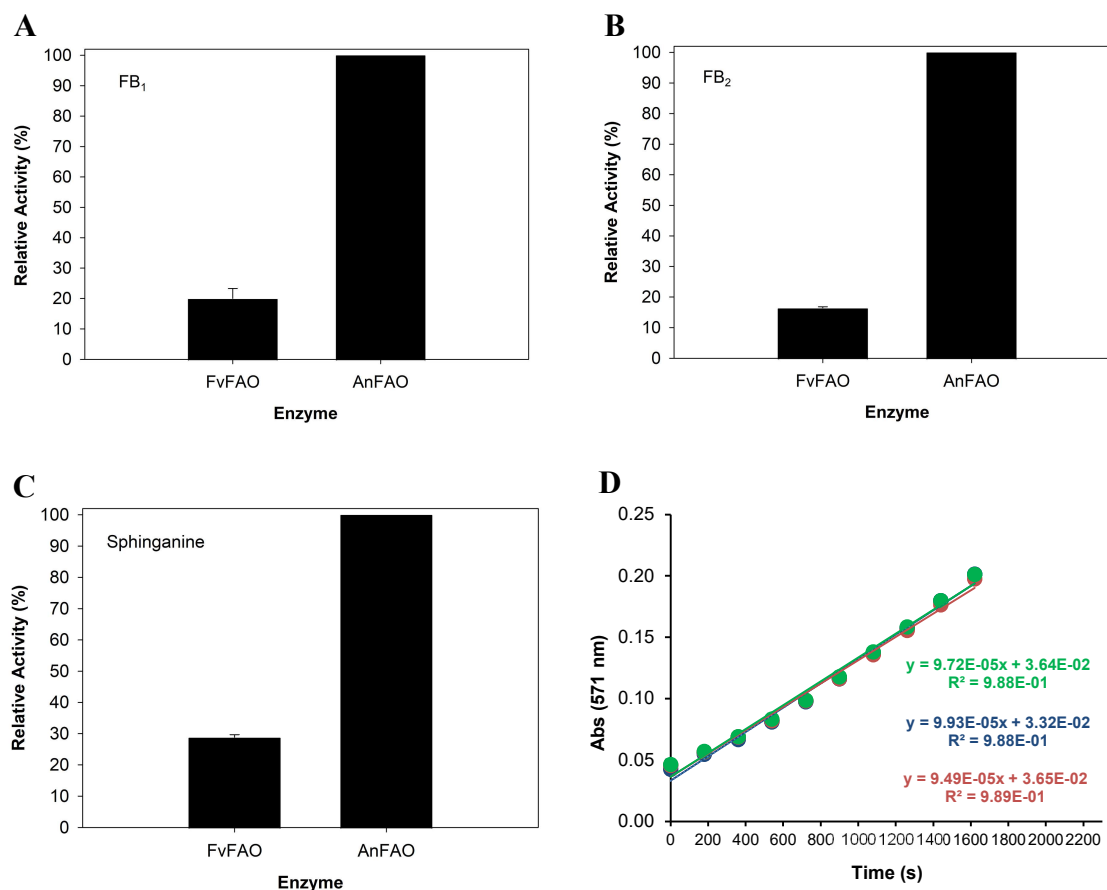


Figure 29. Relative rates for MBP-tagged FvFAO and AnFAO. Each reaction was performed at 37°C with enzyme purified via nickel affinity chromatography followed by size-exclusion chromatography. 50 nM of each MBP-tagged enzyme was used for reactions with FB₁ and FB₂ substrates, and 20 nM enzyme was used for the sphinganine reactions. FB₁ and FB₂ were present at 100 μM in each reaction, and sphinganine at 50 μM. Relative rates were determined using a reaction mixture consisting of the above enzyme and substrate concentrations plus 200 μM AmplexTM Red and 2 U/mL horseradish peroxidase (HRP). Absorbance was measured at 571 nm and used to determine each reaction rate. Relative rates are the means ± SEM of 3 *in vitro* replicates. Relative rates for each enzyme are displayed for three substrates: **A.** FB₁, **B.** FB₂, and **C.** Sphinganine. For

clarity, raw absorbance data is shown for 3 replicates of AnFAO after incubation with FB₂ in **D**.

Table 1. Reaction rates (nM/min) for FvFAO and AnFAO towards FB₁, FB₂, and sphinganine. 50 nM enzyme and 100 μ M substrate were used for the FB₁ and FB₂ reactions. 20 nM enzyme and 50 μ M substrate were used for the sphinganine reactions.

	FB₁	FB₂	Sphinganine
FvFAO	2.53 \pm 0.34	13.30 \pm 0.08	110.80 \pm 3.19
AnFAO	12.74 \pm 0.35	80.72 \pm 1.06	383.66 \pm 0.55

3.5.2 Kinetic Analyses of FvFAO

The following assays were performed with the same MBP-tagged proteins as those above but at constant enzyme concentration and increasing substrate concentrations. Figure 30 shows plots of initial reaction rates at each substrate concentration (A: FB₁ & B: sphinganine). These rates were determined using the slopes of each set of reactions (Figure 30C), and the H₂O₂ standard curve (Figure 30D) was used to convert activity from absorbance/time to molarity/time. The resulting kinetic parameters were calculated using the Michaelis-Menten nonlinear curve fitting model in SigmaPlot and further display FvFAO's relatively poor activity (Table 2). For FB₁, FvFAO's turnover number (k_{cat}) is quite low at 2.22 min⁻¹. It also has a K_M in the low mM range (2.20 mM), indicating a low affinity for this substrate. Taken together, these give an approximate catalytic efficiency (k_{cat}/K_M) of just above 1.00 mM⁻¹ min⁻¹, a value that would be expected to be much higher for FB₂ given the results of the previous relative rate assays.

While extremely inefficient towards FB₁, FvFAO's activity towards sphinganine is much higher in absolute terms, and also closer in comparison to AnFAO. The difference can likely be attributed to the presence of additional functional groups in

FB₁, most notably the TCE sidechains, and their absence in sphinganine. Its turnover number of 24.64 min⁻¹ is much higher for this substrate, reflecting a much higher reaction rate. The micromolar K_M value (0.102 mM) also indicates this enzyme's much higher affinity for sphinganine relative to FB₁. Finally, the catalytic efficiency of FvFAO is over 200 times greater for sphinganine (2.42×10^2 mM⁻¹ min⁻¹), summarizing its preference for this substrate relative to FB₁.

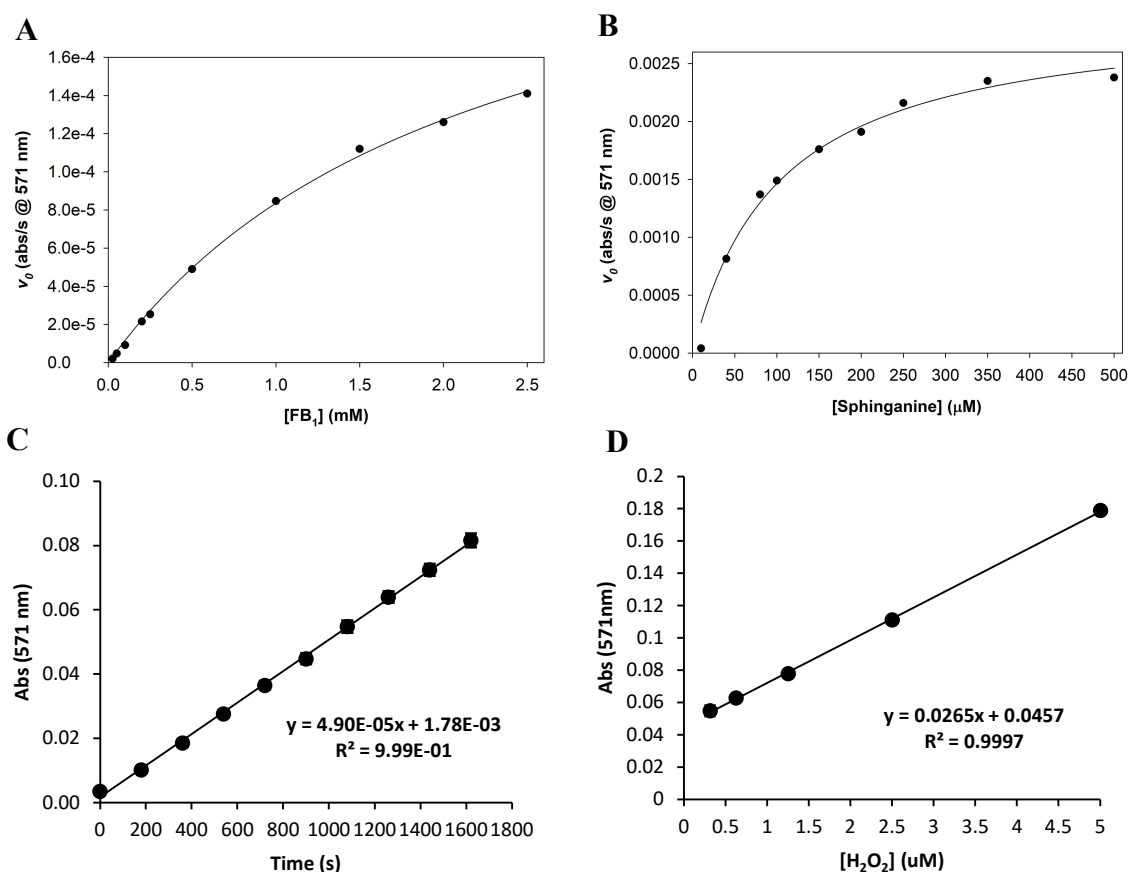


Figure 30. Amplex™ Red Kinetic Assay for FvFAO. Each reaction was performed at 37°C with enzyme purified via nickel affinity chromatography followed by size-exclusion chromatography. 100 nM FvFAO was used for each reaction. FB₁ concentrations ranged from 25 μM to 2.5 mM, and sphinganine from 10 μM to 500 μM. Enzyme velocities were determined using a reaction mixture consisting of the above enzyme and substrate concentrations plus 200 μM Amplex™ Red and 2 U/mL horseradish peroxidase (HRP). Absorbance was measured at 571 nm and used to determine each reaction rate. Velocities for FB₁ (**A**) and sphinganine (**B**) were determined by taking the slope (Abs/s) from assays performed with each substrate concentration. **C.** Raw absorbance data for the 500 μM FB₁

reaction is included for clarity. Absorbance readings are the means \pm SEM of 3 *in vitro* replicates. **D.** H₂O₂ standard curve used to convert reaction rates from Abs/s to μ M/s.

Table 2. Kinetic parameters of FvFAO for FB₁ and sphinganine substrates.

	FB₁	Sphinganine
<i>k</i>_{cat} (min⁻¹)	2.22	24.64
<i>K</i>_M (mM)	2.20 \pm 0.17	0.102 \pm 0.0143
<i>k</i>_{cat}/<i>K</i>_M (mM⁻¹ min⁻¹)	1.01	2.42 \times 10 ²

Chapter 4 – Discussion

The data presented in this thesis ultimately fulfill our primary goal of identifying FLa-generating enzymes, and our secondary goal of characterizing *F. verticillioides*' fumonisin-deaminating activity. While my original aim of identifying the FPy reductase(s) from biological source material was unsuccessful, the switch to our hypothesis-driven approach led to the identification of FUM13 as an enzyme capable of FPy to FLa reduction in both *Aspergilli* and *Fusaria*. This work also indicated that *Fusarium* spp. are capable of generating FPy and FLa fumonisins, which eventually led to the discovery and characterization of the fumonisin-deaminating activity of FvFAO. While FUM13 is already a critical component of the fumonisin biosynthetic pathway, these results indicate it may play a minor role in fumonisin detoxification as well. They also contribute to an explanation for the relatively low amounts of FLa fumonisins present in liquid cultures. Additionally, the discovery of FvFAO's FB-deaminating activity provides a starting point for further research into *Fusarium* spp.' previously unreported ability to detoxify their own fumonisins, and could lead to the development of more biotransformational tools similar to AnFAO.

4.1 Characteristics of FLa-Generating Enzymes

I began by screening various strains of *Aspergilli* to identify those that produce the highest levels of FLa fumonisins. I hypothesized that the highest FLa-generating strains would produce the highest levels of the responsible enzyme. This screening led to a number of promising strains, including MWS1001 and ITEM 11945 (Figure 5-7). Since AnFAO was originally identified in culture supernatants of *A. niger*, we hypothesized that the FPy reductase(s) would be located in the culture supernatant as

well. Therefore, I initially attempted to enrich for FLa-generating activity from this source. Unfortunately, enrichment experiments were ultimately unsuccessful, as we observed no FLa generation in the resuspended culture supernatants after ammonium sulfate precipitation (data not shown). However, this suggested that any FLa-generating enzymes, including FUM13, are not secreted by these fungi. While it is possible the ammonium sulfate precipitation had adverse effects on protein stability, it is likely these enzymes remain intracellular over the duration of the fungal lifespan. Experiments performed by adding ^{13}C -labeled fumonisins to the cultured *Aspergillus* strains also support this notion: no ^{13}C -FLa₂ was observed in culture supernatants after their addition and incubation for up to one week (data not shown). These data suggest that FLa fumonisins may be secreted by the fungi, or that they are released into culture supernatants as fungal metabolism slows and the fungus begins to die. It is also possible that the enzyme(s) are membrane-bound or associated, making their identification from fungal material even more difficult.

This led us to investigate whether lysed fungal cells were capable of FLa-generation. However, after sonicating MWS1001 and ITEM 11945 mycelia, we still did not observe any FLa-generating activity (data not shown). For these reasons, we decided to generate protoplasts in order to more effectively lyse these cells. Protoplasts are fungal cells lacking a cell wall, prepared by incubating mycelia with a mixture of enzymes that break down this organelle^{56,57}. These cells should be much easier to lyse by sonication, as opposed to the dense mats of mycelia that grow in liquid culture. However, after lysis and clarification by centrifugation, there was again no observable FLa generation (Figure 8). There are a number of potential reasons for this lack of activity: again, the FLa-

generating enzyme(s) may be membrane associated and therefore present in the pellet after centrifugation, FPy reduction may be a side reaction for enzymes with natural roles in fumonisin biosynthesis, or it is possible that expression of the FLa-generating enzyme(s) by these fungi is very low.

As a control during our cell wall degradation experiments, we tested the ability of intact protoplasts, which did not undergo lysis by sonication, to generate FLa fumonisins. These results were more promising; we observed conversion of exogenous fumonisin substrates to their FLa forms in fungal cultures using intact protoplasts prepared from MWS1001 (*A. welwitschiae*) mycelia. More specifically, we only observed such conversion after incubation with either FPy₁ or ¹³C-FPy₂ (used to differentiate between the naturally abundant 2 series fumonisins), and not with their corresponding FB forms (Figure 8). These results supported our hypothesis that FLa-generating enzymes use FPy fumonisins, as opposed to FB forms, as their substrates.

While the protoplast assays were promising, they present a unique set of disadvantages as well. Protoplast preparation is very time-consuming, and the amount of cell wall lysing enzymes required to generate a feasible amount of cells would be cost prohibitive. As well, it is possible, if not likely, that the fungal cell wall began regenerating during the 4-day reaction period, raising the question of whether the cells being used were indeed still protoplasts. Lastly, it is still unclear where exactly the FLa-generating activity comes from within the protoplasts, since cell lysis suggested that the enzyme(s) are not contained in the cytoplasm. Whether the enzyme(s) are indeed membrane associated or if they are simply expressed at low levels, the protoplasts' poor FLa-generating activity make it unfeasible to enrich for and identify the enzyme(s) from

this source material. Given these limitations, we decided to shift our focus to *in vitro* assays with recombinant enzymes from the SDR superfamily that we hypothesized may be responsible for FLa production.

Our investigation of *A. niger* sdr1 is, in part, what led us to hypothesize that (an) enzyme(s) from the SDR superfamily is/are responsible for FLa production. sdr1 is a gene of unknown function within the *Aspergillus* fumonisin biosynthetic gene cluster, but absent in *Fusaria*¹⁸. The putative function of SDR enzymes is to catalyze carbonyl-alcohol oxidoreduction reactions, and members of this family participate in many types of primary and secondary metabolism⁵⁸. Therefore, sdr1 seemed a logical candidate to reduce FPy carbonyl groups to the hydroxyls in FLa fumonisins. Unfortunately, this protein proved difficult to work with *in vitro* and was ultimately unable to generate FLa fumonisins when administered FB or FPy substrates. However, this led us to investigate other fungal SDR proteins, one of which is FUM13, which catalyzes the oxidoreduction of a fumonisin intermediate similar in structure to FPy fumonisins⁴⁹. All SDR enzymes are NAD(P)H-dependent oxidoreductases, and FUM13 specifically uses NADPH as a cofactor during fumonisin biosynthesis^{49,58,59}. It was for these reasons that NADPH was included as a cofactor in the assays for both *A. niger* and *F. verticillioides* FUM13 at a concentration of 50 μ M; the same used by Yi *et al.* when elucidating the native function of the *F. verticillioides* isoform.

FUM13's newly discovered ability to inefficiently reduce FPy fumonisins might also explain the low FLa levels observed in liquid cultures and in our protoplast assays. That is, the reduction of FPy fumonisins to FLa forms is likely a side reaction for this biosynthetic enzyme, rather than a function that evolved in parallel. During our

protoplast experiments we observed very low FLa levels, which corresponds to the inefficient reduction of the FPy forms after incubation with recombinant *A. niger* and *F. verticillioides* FUM13 (Figure 19 & 22). While we did observe up to 75% conversion of FPy₁ and nearly 99% of FPy₂ to their FLa forms by *F. verticillioides* FUM13 in one instance, the protein concentration was relatively high (~13 μM) and the substrate concentration quite low (~0.6 μM) (Figure 24). We then lowered the enzyme concentration to 100 nM and 1 μM, and tested each with increased substrate concentrations of 5.6 μM, 28 μM, and 56 μM to see if the enzyme remained as effective (Figure 25). However, its conversion efficiency dropped dramatically: at 100 nM, *F. verticillioides* FUM13 was unable to reduce FPy₁ or FPy₂ at any of the concentrations added (data not shown), while at 1 μM its conversion efficiency ranged between only ~2% (56 μM FPy₁) and ~10% (5.6 μM FPy₂).

As mentioned, this is likely because neither *A. niger* nor *F. verticillioides* FUM13 evolved for the purpose of reducing FPy carbonyl groups to the hydroxyls in the FLa forms. While similar, the structure of FUM13's native substrate differs considerably compared to FPy₁ and FPy₂ (Figure 17B)^{17,49}. The most striking difference between this intermediate and the FPy forms is that it lacks the two large TCE groups which are added to the FB form scaffold near the end of the biosynthetic process. This suggests that the FUM13 active site is too small to accommodate these groups comfortably, and that its shape is not entirely complimentary to either FPy₁ or FPy₂. Additionally, while FLa fumonisins are slightly less toxic than the FPy forms, these deaminated fumonisins are already dramatically less toxic than their FB counterparts⁴⁷. This further contributes to an explanation of why FLa levels are so low in fungal liquid culture, and why FPy reduction

by FUM13 is so inefficient: *Aspergilli* are likely sufficiently protected from fumonisin toxicity after the deamination step alone.

Notably, both *A. niger* and *F. verticillioides* FUM13 appear to prefer FPy₂ as a substrate over FPy₁. *Aspergilli* do not produce FB₁ fumonisins and AnFAO prefers FB₂ as a substrate over FB₁, therefore it makes sense that *A. niger* FUM13 follows the same trend and more efficiently reduces FPy₂⁴⁸. However, *F. verticillioides* generally produces considerably higher levels of FB₁ fumonisins compared to FB₂, so we expected it to prefer FPy₁ as a substrate over FPy₂. There is only a single difference in the structure/chemical composition of FPy₁ and FPy₂, and it occurs at the R₅ position denoted in Figure 3. FPy₁ contains a hydroxyl group at this position, as opposed to a hydrogen in FPy₂. It is likely that this extra OH group in FPy₁ partially hinders its entrance into FUM13's active site, whereas the smaller H in FPy₂ allows for easier binding and catalysis.

4.2 Fumonisin Detoxification in *Aspergilli* vs. *Fusaria*: Newly Discovered Enzymes & Functions lead to New Questions

As previously discussed, many fungi resist the toxic effects of their mycotoxins through biotransformation and other means. For example, several *Fusarium* spp. contain genes, *TRI101* and *TRI201*, that encode 3-O-acetyltransferases responsible for acetylating the C-3 hydroxyl group on trichothecene molecules, such as DON, significantly reducing their toxicity⁶⁰⁻⁶². *A. niger* and *A. welwitschiae*'s fumonisin deamination and reduction capabilities have also been discussed at length in this thesis. On the other hand, *F. verticillioides* contains genes within its fumonisin biosynthetic gene cluster that likely compensate for the FB-mediated competitive inhibition of ceramide

synthase (FUM17 & FUM18 – further discussion below)⁴⁴⁻⁴⁶. However, as previously mentioned, FPy and FLA production by *Fusarium* spp. has never been reported in the literature. In fact, production of these compounds by *Aspergilli* was only first reported as recently as 2015^{21,47,63}. We have now generated data that indicates FPy and FLA production by a *Fusarium* species in liquid culture for the first time, while also identifying enzymes from *F. verticillioides* that are capable of deaminating FB fumonisins (FvFAO) and reducing FPy forms (FUM13). The FPy and FLA amounts produced by *F. verticillioides* in the lab are relatively low compared to the FB forms, with FLA₂ being the highest at ~10-fold lower than FB₂, and FLA₁ being the lowest at ~200-fold lower than FB₁ (Figure 26). However, these discoveries raise a number of questions regarding the differences in fumonisin detoxification and protection methods in *Aspergilli* and *Fusaria*. They also provide a starting point for future research into the similarities and differences in fumonisin metabolism as a whole between these two genera.

This analysis can begin by comparing the two sets of enzymes in question: AnFAO and FvFAO for FB deamination, and the *A. niger* and *F. verticillioides* FUM13 isoforms for FPy reduction. FvFAO is AnFAO's most similar homolog in *F. verticillioides*, so these two enzymes are generally quite similar: they are both MAOs, they consist of 474 and 464 amino acids, respectively, and they each have an approximate molecular weight of 51 kDa. However, a multiple sequence alignment by Clustal Omega shows a percent identity of 44.71%.

This large difference at the amino acid level surely contributes to the difference in activity between these two enzymes, which is very apparent when

comparing their kinetic parameters, especially towards FB₁ (Figure 30 & Table 2). AnFAO's turnover number (8.7 min⁻¹) is ~4 times greater for FB₁, and its K_M (390.6 μM) is almost 6 times lower, indicating both a higher affinity and reaction rate than FvFAO⁴⁸. This comparison can be summarized by evaluating their catalytic efficiencies, where AnFAO's is over 20 times greater than FvFAO's (22.27 mM⁻¹ min⁻¹ vs. 1.01 mM⁻¹ min⁻¹). On the other hand, even though AnFAO also deaminates sphinganine more efficiently, FvFAO's catalytic efficiency is only ~5 times lower for this substrate (1.17×10³ mM⁻¹ min⁻¹ vs. 2.42×10² mM⁻¹ min⁻¹). However, when comparing FvFAO's catalytic efficiencies for FB₁ and sphinganine (>200-fold difference), it is clear that this enzyme prefers sphinganine as a substrate over FB₁ to a greater extent than AnFAO (~50-fold difference). This comparison suggests that FvFAO's potential development into a tool for fumonisin detoxification may prove difficult, as it has greater relative activity than AnFAO towards this unwanted substrate.

When AnFAO was identified, substitutions at amino acid position 323 were found to be critical for fumonisin deamination activity. In particular, an asparagine to aspartate substitution at this position lowered enzyme activity towards FB₂ by 82% (wild type AnFAO as referred to in this thesis contains an asparagine at position 323)^{48,72}. FvFAO contains a glutamate at the equivalent position (residue 329), and we expect that making an analogous mutation (E329N) would increase enzyme activity. As such, immediate future work with FvFAO could involve mutagenesis experiments followed by Amplex™ Red assays to compare its activity to the wild type version and to AnFAO.

While the above comparisons provide valuable information for future work with FvFAO, it is also important to consider two limitations associated with them. First,

FvFAO's kinetic parameters for FB₁ are likely misestimated due to the substrate concentrations used in the assay. The initial rate plot in Figure 30A does not fully plateau at the highest FB₁ concentrations used, meaning that the k_{cat} is a presumed underestimate and the K_M an overestimate. Higher concentrations were not used due to limited substrate availability, however future assays could indicate a greater efficiency towards FB₁ than reported in this thesis. Additionally, we did not determine FvFAO's kinetic parameters for FB₂ because of the cost prohibitive nature of this compound. However, it is clear from the relative rate assays that FvFAO prefers FB₂ as a substrate over FB₁, and performing an additional kinetic analysis with this compound may result in parameters more comparable to AnFAO.

Naturally, like the above MAO homologs, *A. niger* and *F. verticillioides* FUM13 also share many similarities: they are both SDRs, they contain 349 and 369 amino acids, respectively, and their molecular weights range between approximately 38 and 40 kDa. However, a Clustal Omega multiple sequence alignment showed a similar result to FvFAO and AnFAO: the FUM13 isoforms share a percent identity of 48.55%. Once again, this considerable difference at the amino acid level is likely responsible for the difference in activity between the two enzymes. Based on percent conversion in the LC-MS assays, *F. verticillioides* FUM13 was up to 75% more active than the *A. niger* isoform towards FPy₁, and up to 97% more active for FPy₂ (Figures 19 & 24). However, future experiments at equivalent enzyme and substrate concentrations should be performed to obtain a more accurate comparison of the activity of these isoforms.

In addition to these interspecies differences, sequence variation between the same enzymes in separate strains of *A. niger*, *A. welwitschiae*, and *F. verticillioides* is

very common. For example, the *sdr1* homologs from *A. niger* discussed in section 3.3.1 shared a percent identity of 97.58%. Moreover, based on a BLAST search of the *A. niger* FUM13 isoform analyzed in this thesis, there are homologs in other strains of *A. niger* that have percent identities as low as 97.42%. While this divergence in sequence identity is minor, small variations in amino acid composition can lead to striking differences in enzyme activity, as seen with the asparagine/aspartate substitution at position 323 in AnFAO^{48,72}. This intraspecies variation may help explain the varying levels of fumonisin production, not only FLA forms, between the different strains of *Aspergilli* screened in section 3.1 as well (Figure 5-7). Even a single amino acid substitution in their FPy- and FLA-generating enzymes could significantly alter their efficiency. Testing the activity of the FUM13 homologs from the BLAST search above could help prove this hypothesis as well.

In addition to interspecies differences at the enzyme level, there are important differences between the fumonisin BGCs of *A. niger/welwitschiae* and *F. verticillioides* that may also help explain the different fumonisin protection methods employed by these two genera (Figure 2). All the genes in the *Aspergillus* spp. fumonisin BGC are also present in their *F. verticillioides* counterpart, except for *sdr1*. We have now established *in vitro* that FUM13 is at least partially responsible for FPy reduction in each of these species, however it remains possible that *sdr1* has a similar function. While results obtained in this thesis suggest this protein does not play a role in FPy reduction, further research involving optimized expression and purification methods may be useful to definitively rule out this possibility. This protein is unique to the *Aspergillus* fumonisin BGC, it is a member of the SDR superfamily, and *Aspergilli* do not appear to compensate

for the toxicity of their own fumonisins other than by deamination and reduction of the FB and FPy forms. And while this protein proved difficult to study *in vitro*, it remains possible that it shares a similar role to FUM13's newfound function when expressed in *Aspergilli*.

Even more telling in the analysis of fumonisin protection in *Aspergilli* and *Fusaria* is the presence of FUM17 and FUM18 in the *F. verticillioides* fumonisin BGC, and their absence in *Aspergilli* (Figure 2). As briefly discussed, these genes are responsible for the expression of two ceramide synthases; the enzyme inhibited by FB fumonisins in sphinganine biosynthesis⁴⁴⁻⁴⁶. Their expression may help explain why *F. verticillioides* does not rely on post-biosynthetic modification of FB fumonisins to protect themselves. It is presumed that these genes encode additional versions of the enzyme to compensate for inhibition of their native forms. Indeed, researchers have shown that FUM18 knockout strains of *F. verticillioides* exhibit decreased fitness in the presence of FB₁, especially during spore germination when cells are actively dividing⁴⁶. Researchers have also postulated that FUM17 assists in fumonisin protection by forming heterodimers with CER3 (a ceramide synthase gene outside the fumonisin BGC), which is supported by previous research identifying heterodimers of ceramide synthase within the yeast ceramide synthase complex^{46,64}.

Interestingly, Janevska *et al.*'s study of *F. verticillioides* FUM19 knockout strains suggests that this gene product may also play a role in fumonisin protection. The role of this ABC transporter gene in FB₁ export is still up for debate, however after knocking it out in a Δ FUM21 background (a transcription factor that regulates expression of other FUM genes), the researchers observed an upregulation of both FUM17 and

FUM18. This suggested to them that FUM19 is a key component in a negative feedback loop regulating FB₁ levels in *F. verticillioides*, which is further supported by previous studies demonstrating increased fungal secondary metabolite synthesis upon deletion of equivalent ABC transporter genes^{46,65–67}. This potential self-defense role of FUM19 makes the differences in fumonisin protection systems between *Aspergilli* and *Fusaria* even more interesting. FUM19 is also present in the *Aspergillus* fumonisin BGC, therefore it may complement the protection provided by AnFAO and, possibly, FUM13. Further research on the role of this gene product in *Aspergilli* may give more insight into potential similarities in fumonisin protection methods between *Aspergilli* and *Fusaria*. Monitoring fitness, fumonisin production, and gene expression in FUM19 knockouts of *Aspergillus* spp. may be of interest, especially since they lack the FUM17 and FUM18 genes. It would be particularly intriguing to monitor the impact of such deletions on the expression of native ceramide synthase genes in *Aspergilli*.

4.3 Conclusions and Future Directions

Overall, the identification of FP_Y-reducing enzymes, along with the discovery of *F. verticillioides*' capability to post-biosynthetically modify their fumonisins, expands our growing knowledge of fumonisin metabolism in *Aspergilli* and *Fusaria*. Excitingly, these results also provide a starting point for the development of new biotransformational tools that could be used to mitigate fumonisin contamination in food and feed. While its FP_Y-reducing activity is quite low, *F. verticillioides* FUM13 has the potential for improvement and use as a tool for more comprehensive fumonisin detoxification. Possibly more exciting, FvFAO provides an even better starting point for new tools. *F. verticillioides* poses the greatest agro-economic threat with regards to

fumonisin contamination, moreso than *Aspergilli*. This problem makes our discovery of this species' novel detoxification abilities even more valuable. Further investigation into the fumonisin deamination mechanisms in *Fusarium* spp. could lead to the development of recombinant MAOs that more efficiently deaminate FB₁, the most toxic and widely produced fumonisin. This would address the greatest challenge faced with AnFAO; its relatively low deamination activity towards FB₁, especially compared to FB₂⁴⁸. Currently, FvFAO is considerably less efficient at deaminating fumonisins than AnFAO, being ~5-fold less active for both FB₁ and FB₂ (Figure 29). However, as previously described, AnFAO's activity changed significantly with substitutions at amino acid position 323, and designing an E329N mutant of FvFAO should increase its activity.

The Garnham lab has found success in increasing the activity of AnFAO through targeted mutagenesis, generating a suite of mutants with increased activity. Similar experiments with FvFAO would ideally be performed after solving the structure of this protein by x-ray crystallography. Given its promising expression pattern in *E. coli*, its relatively high solubility, and its favourable behaviour during purification, this protein appears to be a suitable candidate for crystal formation. Solving its structure would allow for detailed analysis of its active site, making rational mutant design much simpler. Some of the immediate mutations worth exploring could involve increasing the size of the binding pocket to accommodate the large TCE sidechains; mutations analogous to those made for the AnFAO mutants with increased activity. Alternatively, random mutagenesis of select regions of FvFAO could be performed in a high-throughput manner to increase its activity towards FB₁. Dr. Patrick Telmer has recently developed a colourimetric, plate-based FB deamination assay using Amplex™ Red in a similar approach to our relative

rate and kinetic assays. We are able to generate large, randomized mutant libraries of AnFAO using Megaprimer PCR of Whole Plasmid (MEGAWHOP) methodology before transforming them into *E. coli* and monitoring colour changes on LB agar plates containing either FB₁ or FB₂⁶⁸. Presuming FvFAO's baseline activity can be increased with the E329N mutation sufficiently enough to obtain reliable colour changes, this assay could be used to identify mutants with increased activity for this enzyme as well.

Similar future experiments could also be performed with FUM13. Firstly, no structure has been solved for either the *F. verticillioides* or *A. niger* homologs. Given the promising expression pattern and purification results for the *F. verticillioides* isoform, future work could begin by attempting crystal formation and x-ray diffraction. Gaining structural information for this protein would give valuable insight to the size and shape of its active site, allowing for rational mutant design with the goal of modifying its binding pocket to more readily accommodate the large TCE sidechains on FPy₁ and FPy₂. It would also be interesting to generate FUM13 knockouts of *F. verticillioides* and *A. niger* and monitor changes in FLa production, however this would not be possible since FUM13 is required for fumonisin biosynthesis. Alternatively, we could perform *in vitro* experiments with a catalytically dead mutant of the enzyme as a control to support the conclusion that it is in fact reducing FPy fumonisins following our hypothesized mechanism. As a member of the SDR superfamily, FUM13 contains a Y-X-X-X-K catalytic motif, where the tyrosine and lysine are crucial for catalysis: eliminating one should theoretically inactivate the enzyme⁶⁹⁻⁷¹. This motif is located between position 176-180 in *F. verticillioides* FUM13. Therefore, a catalytically dead mutant could be generated with a Y176F mutation. We would expect this mutant to be completely

incapable of reducing FPy fumonisins, and it could possibly be used for x-ray crystallography as well. For example, a Y176F mutant could be used to solve a structure of this protein bound to its native fumonisin-intermediate substrate, FPy₁, FPy₂, or even hydrolyzed fumonisins where the TCE sidechains have been removed. Again, a structure of this type would provide information on how to modify the active site such that it is better able to bind and reduce FPy fumonisins.

While both FUM13 isoforms provided promising FLA-generation data, it remains possible that *sdr1* also plays a role in FPy reduction in *Aspergilli*. As previously mentioned, further experiments involving additional expression and purification techniques may lead to more conclusive data for this protein. For example, alternative expression systems could lead to more favourable induction and solubility patterns. The Menassa lab at AAFC commonly uses tobacco plants to express recombinant proteins, and it is possible that expressing *sdr1* in such a system may improve solubility and folding due to the presence of protein chaperones and post-translational modifications that may be absent in BL21 *E. coli*. Future experiments could also involve exploring additional buffer components and concentrations via thermal shift assays to increase protein solubility. The Junop lab at Western has access to Durham pH and Salt Screen kits (Molecular Dimensions, England) that contain 96 different buffer and salt conditions, respectively. Each of these can be incubated separately with a purified protein to determine its preferred buffer components in a high-throughput manner. Along with each screening condition, SYPRO Orange Protein Stain (Thermo Scientific, United States) is added to the sample before running in a real-time PCR machine. This dye binds hydrophobic amino acids usually buried in the core of a protein, and its change in

fluorescence can be plotted at increasing temperatures to generate a melting curve for each condition. The buffer and salt components that result in the highest T_m for the protein of interest can then be used to create optimized lysis and purification buffers.

Along with working to improve *sdr1*'s expression and solubility, generating *sdr1* knockout strains of *Aspergilli* may also provide information on the native function of this protein. Future experiments could involve knocking out the *sdr1* gene in MWS1001 and ITEM 11945, for example, and monitoring their fitness and FLA production relative to the wild type strains. It would be valuable to see whether or not fitness is impacted in the knockout strains, and if they produce lower levels of FLA fumonisins than their wild type counterparts. Overall, there are a number of potential avenues that could be explored to definitively rule out the role of *sdr1* in FLA production by *Aspergilli*.

In summary, I was able to identify an enzyme, FUM13, from *A. niger* and *F. verticillioides* capable of FLA generation, while also characterizing an *F. verticillioides* MAO, FvFAO, that deaminates FB fumonisins. *F. verticillioides* FvFAO and FUM13 are the first enzymes reported to be capable of post-biosynthetic fumonisin modification in *Fusaria*. FvFAO in particular presents an exciting starting point for the development of new biotransformational tools to mitigate fumonisin contamination of agricultural food and feed products. Similarly, the discovery of FUM13's ability to reduce FPY fumonisins opens new avenues for researchers to investigate the differences in fumonisin protection systems between *Aspergilli* and *Fusaria*.

References

1. Bennett, J. W. Mycotoxins, mycotoxicoses, mycotoxicology and mycopathologia. *Mycopathologia* **100**, 3–5 (1987).
2. Zain, M. E. Impact of mycotoxins on humans and animals. *J. Saudi Chem. Soc.* **15**, 129–144 (2011).
3. Berthiller, F. *et al.* Masked mycotoxins: A review. *Mol. Nutr. Food Res.* **57**, 165–186 (2013).
4. Richard, J. L. Some major mycotoxins and their mycotoxicoses—An overview. *Int. J. Food Microbiol.* **119**, 3–10 (2007).
5. Eskola, M. *et al.* Worldwide contamination of food-crops with mycotoxins: Validity of the widely cited ‘FAO estimate’ of 25%. *Crit. Rev. Food Sci. Nutr.* **60**, 2773–2789 (2020).
6. Robens, J. F. & Richard, J. L. Aflatoxins in animal and human health. *Rev. Environ. Contam. Toxicol.* **127**, 69–94 (1992).
7. Goyarts, T., Grove, N. & Dänicke, S. Effects of the Fusarium toxin deoxynivalenol from naturally contaminated wheat given subchronically or as one single dose on the in vivo protein synthesis of peripheral blood lymphocytes and plasma proteins in the pig. *Food Chem. Toxicol.* **44**, 1953–1965 (2006).
8. Islam, M. N. *et al.* Naturally occurring Fusarium species and mycotoxins in oat grains from Manitoba, Canada. *Toxins (Basel)*. **44**, 670 (2021).
9. Hidy, P. H., Baldwin, R. S., Greasham, R. L., Keith, C. L. & McMullen, J. R. Zearalenone and Some Derivatives: Production and Biological Activities. *Adv. Appl. Microbiol.* **22**, 59–82 (1977).
10. Pfohl-Leszkowicz, A., Petkova-Bocharova, T., Chernozemsky, I. N. & Castegnaro, M. Balkan endemic nephropathy and associated urinary tract tumours: A review on aetiological causes and the potential role of mycotoxins. *Food Addit. Contam.* **19**, 282–302 (2002).
11. Miller, J. D. Changing patterns of fungal toxins in crops: Challenges for analysts. *J. AOAC Int.* **99**, 837–841 (2016).
12. Susca, A. *et al.* Variation in fumonisin and ochratoxin production associated with differences in biosynthetic gene content in *Aspergillus niger* and *A. welwitschiae* isolates from multiple crop and geographic origins. *Front. Microbiol.* **7** (2016).
13. Kamle, M. *et al.* Fumonisin: Impact on agriculture, food, and human health and their management strategies. *Toxins (Basel)*. **11**, 328 (2019).
14. Palumbo, J. D., O’Keeffe, T. L., Quejarro, B. J., Yu, A. & Zhao, A. Comparison of *Aspergillus* section Nigri species populations in conventional and organic raisin vineyards. *Curr. Microbiol.* **76**, 848–854 (2019).
15. Testempasis, S. I., Kamou, N. N., Papadakis, E. N., Menkissoglu-Spiroudi, U. & Karaoglanidis, G. S. Conventional vs. organic vineyards: Black *Aspergilli*

- population structure, mycotoxigenic capacity and mycotoxin contamination assessment in wines, using a new Q-TOF MS-MS detection method. *Food Control* **136**, 108860 (2022).
16. Miller, J. D. Factors that affect the occurrence of fumonisin. *Environ. Health Perspect.* **109**, 321–324 (2001).
 17. Alexander, N. J., Proctor, R. H. & McCormick, S. P. Genes, gene clusters, and biosynthesis of trichothecenes and fumonisins in *Fusarium*. *Toxin Rev.* **28**, 198–215 (2009).
 18. Susca, A. *et al.* Variation in the fumonisin biosynthetic gene cluster in fumonisin-producing and nonproducing black aspergilli. *Fungal Genet. Biol.* **73**, 39–52 (2014).
 19. Branham, B. E. & Plattner, R. D. Alanine is a precursor in the biosynthesis of fumonisin B₁ by *Fusarium moniliforme*. *Mycopathologia* **124**, 99–104 (1993).
 20. ApSimon, J. W. Structure, synthesis, and biosynthesis of fumonisin B₁ and related compounds. *Environ. Health Perspect.* **109**, 245–249 (2001).
 21. Renaud, J. B., Kelman, M. J., Qi, T. F., Seifert, K. A. & Sumarah, M. W. Production filtering with rapid polarity switching for the detection of all fumonisins and AAL-toxins. *Rapid Commun. Mass Spectrom.* **29**, 2131–2139 (2015).
 22. Bezuidenhout, S. C. *et al.* Structure elucidation of the fumonisins, mycotoxins from *Fusarium moniliforme*. *J. Chem. Soc. Chem. Commun.* **1730**, 743–745 (1988).
 23. Branham, B. E. & Plattner, R. D. Isolation and characterization of a new fumonisin from liquid cultures of *Fusarium moniliforme*. *J. Nat. Prod.* **56**, 1630–1633 (1993).
 24. Merrill, A. H., Sullards, M. C., Wang, E., Voss, K. A. & Riley, R. T. Sphingolipid metabolism: Roles in signal transduction and disruption by fumonisins. *Environ. Health Perspect.* **109**, 283–289 (2001).
 25. Riley, R. T. *et al.* Sphingolipid perturbations as mechanisms for fumonisin carcinogenesis. *Environ. Health Perspect.* **109**, 301–308 (2001).
 26. Rehman, F. U. *et al.* Seed-borne fungal diseases of maize (*Zea mays* L.): A review. *Agrinula J. Agroteknologi dan Perkeb.* **4**, 43–60 (2021).
 27. Kellerman, T. S. *et al.* Leukoencephalomalacia in two horses induced by oral dosing of fumonisin B₁. *Onderstepoort J. Vet. Res.* **57**, 269–275 (1990).
 28. Harrison, L. R., Colvin, B. M., Greene, J. T., Newman, L. E. & Cole, J. R. Pulmonary edema and hydrothorax in swine produced by fumonisin B₁, a toxic metabolite of *fusarium moniliforme*. *J. Vet. Diagnostic Investig.* **2**, 217–221 (1990).
 29. Marasas, W. F. O. *et al.* Fumonisins disrupt sphingolipid metabolism, folate transport, and neural tube development in embryo culture and in vivo: A potential risk factor for human neural tube defects among populations consuming

- fumonisin-contaminated maize. *J. Nutr.* **134**, 711–716 (2004).
30. Rheeder, J. P. *et al.* Fusarium moniliforme and fumonisins in corn in relation to human esophageal cancer in Transkei. *Phytopathology.* **82**, 353–357 (1992).
 31. Sammon, A. M. Cancer of the oesophagus in africa, population susceptibility, and preventive intervention: A literature review. *Glob. J. Health Sci.* **13**, 124 (2021).
 32. Rachaputi, N. R., Wright, G. C. & Krosch, S. Management practices to minimise pre-harvest aflatoxin contamination in Australian peanuts. *Aust. J. Exp. Agric.* **42**, 595–605 (2002).
 33. Lanyasunya, T., Wamae, T., Musa, H. H., Olowofeso, O. & Lokwaleput, I. K. The risk of mycotoxins contamination in dairy feed and milk on smallholder dairy farms in Kenya. *Pakistan J. Nutr.* **4**, 162–169 (2005).
 34. Cleveland, T. E., Dowd, P. F., Desjardins, A. E., Bhatnagar, D. & Cotty, P. J. United States Department of Agriculture - Agricultural Research Service research on pre-harvest prevention of mycotoxins and mycotoxigenic fungi in US crops. *Pest Manag. Sci.* **59**, 629–642 (2003).
 35. Dorner, J. W. & Cole, R. J. Effect of application of nontoxigenic strains of *Aspergillus flavus* and *A. parasiticus* on subsequent aflatoxin contamination of peanuts in storage. *J. Stored Prod. Res.* **38**, 329–339 (2002).
 36. Wang, J. S. *et al.* Short-term safety evaluation of processed calcium montmorillonite clay (NovaSil) in humans. *Food Addit. Contam.* **22**, 270–279 (2005).
 37. Hathout, A. S. & Aly, S. E. Biological detoxification of mycotoxins: A review. *Ann. Microbiol.* **64**, 905–919 (2014).
 38. Rodriguez, H. *et al.* Degradation of ochratoxin a by *brevibacterium* species. *J. Agric. Food Chem.* **59**, 10755–10760 (2011).
 39. Yeh, H. H. *et al.* Resistance gene-guided genome mining: Serial promoter exchanges in *Aspergillus nidulans* reveal the biosynthetic pathway for fellutamide B, a proteasome inhibitor. *ACS Chem. Biol.* **11**, 2275–2284 (2016).
 40. Cole, R. J., Kirksey, J. W. & Blankenship, B. R. Conversion of aflatoxin B₁ to isomeric hydroxy compounds by *Rhizopus* spp. *J. Agric. Food Chem.* **20**, 1100–1102 (1972).
 41. Faraj, M. K., Smith, J. E. & Harran, G. Aflatoxin biodegradation: effects of temperature and microbes. *Mycol. Res.* **97**, 1388–1392 (1993).
 42. Varga, J., Péteri, Z., Tábori, K., Téren, J. & Vágvölgyi, C. Degradation of ochratoxin A and other mycotoxins by *Rhizopus* isolates. *Int. J. Food Microbiol.* **99**, 321–328 (2005).
 43. Varga, J. & Tóth, B. Novel strategies to control mycotoxins in feeds: A review. *Acta Vet. Hung.* **53**, 189–203 (2005).
 44. Proctor, R. H., Brown, D. W., Plattner, R. D. & Desjardins, A. E. Co-expression of 15 contiguous genes delineates a fumonisin biosynthetic gene cluster in *Gibberella*

- moniliformis. *Fungal Genet. Biol.* **38**, 237–249 (2003).
45. Li, T., Su, X., Qu, H., Duan, X. & Jiang, Y. Biosynthesis, regulation, and biological significance of fumonisins in fungi: current status and prospects. *Crit. Rev. Microbiol.* **48**, 1–13 (2021).
 46. Janevska, S. *et al.* Self-protection against the sphingolipid biosynthesis inhibitor fumonisin B₁ is conferred by a FUM cluster-encoded ceramide synthase. *MBio* **11**, e00455-20 (2020).
 47. Burgess, K. M. N., Renaud, J. B., McDowell, T. & Sumarah, M. W. Mechanistic insight into the biosynthesis and detoxification of fumonisin mycotoxins. *ACS Chem. Biol.* **11**, 2618–2625 (2016).
 48. Garnham, C. P. *et al.* Identification and characterization of an *Aspergillus niger* amine oxidase that detoxifies intact fumonisins. *J. Agric. Food Chem.* **68**, 13779–13790 (2020).
 49. Yi, H., Bojja, R. S., Fu, J. & Du, L. Direct evidence for the function of FUM13 in 3-ketoreduction of mycotoxin fumonisins in *Fusarium verticillioides*. *J. Agric. Food Chem.* **53**, 5456–5460 (2005).
 50. Tanaka, N., Nonaka, T., Nakamura, K. & Hara, A. SDR structure, mechanism of action, and substrate recognition. *Curr. Org. Chem.* **5**, 89–111 (2005).
 51. Lichman, B. R. *et al.* Uncoupled activation and cyclization in catmint reductive terpenoid biosynthesis. *Nat. Chem. Biol.* **15**, 71–79 (2019).
 52. Hosfield, D. J. *et al.* Conformational flexibility in crystal structures of human 11 β -hydroxysteroid dehydrogenase type I provide insights into glucocorticoid interconversion and enzyme regulation. *J. Biol. Chem.* **280**, 4639–4648 (2005).
 53. Wierenga, R. K., de Jong, R. J., Kalk, K. H., Hol, W. G. J. & Drenth, J. Crystal structure of p-hydroxybenzoate hydroxylase. *J. Mol. Biol.* **131**, 55–73 (1979).
 54. Schreuder, H. A., van der Laan, J. M., Hol, W. G. J. & Drenth, J. Crystal structure of p-hydroxybenzoate hydroxylase complexed with its reaction product 3,4-dihydroxybenzoate. *J. Mol. Biol.* **199**, 637–648 (1988).
 55. Gaweska, H. & Fitzpatrick, P. F. Structures and mechanism of the monoamine oxidase family. *Biomol. Concepts* **2**, 365–377 (2011).
 56. Son, Y. E. & Park, H. S. Genetic manipulation and transformation methods for *Aspergillus* spp. *Mycobiology* **49**, 95–104 (2020).
 57. Peberdy, J. F. Fungal Protoplasts. in *The Mycota* (ed. Kück, U.) 49–60 (Springer, 1995).
 58. Tonfack, L. B. *et al.* The plant SDR superfamily: Involvement in primary and secondary metabolism. *Curr. Top. Plant Biol.* **12**, 41–53 (2011).
 59. Katzberg, M., Skorupa-Parachin, N., Gorwa-Grauslund, M. F. & Bertau, M. Engineering cofactor preference of ketone reducing biocatalysts: A mutagenesis study on a γ -diketone reductase from the yeast *saccharomyces cerevisiae* serving as an example. *Int. J. Mol. Sci.* **11**, 1735–1758 (2010).

60. Venkatesh, N. & Keller, N. P. Mycotoxins in conversation with bacteria and fungi. *Front. Microbiol.* **10**, 1–10 (2019).
61. Kimura, M. *et al.* Trichothecene 3-O-acetyltransferase protects both the producing organism and transformed yeast from related mycotoxins. *J. Biol. Chem.* **273**, 1654–1661 (1998).
62. Khatibi, P. A. *et al.* Bioprospecting for trichothecene 3-O-acetyltransferases in the fungal genus *Fusarium* yields functional enzymes with different abilities to modify the mycotoxin deoxynivalenol. *Appl. Environ. Microbiol.* **77**, 1162–1170 (2011).
63. Qi, T. F. *et al.* Diversity of mycotoxin-producing black Aspergilli in Canadian vineyards. *J. Agric. Food Chem.* **64**, 1583–1589 (2016).
64. Vallée, B. & Riezman, H. Lip1p: A novel subunit of acyl-CoA ceramide synthase. *EMBO J.* **24**, 730–741 (2005).
65. Janevska, S. *et al.* Gibepyrone biosynthesis in the rice pathogen *Fusarium fujikuroi* is facilitated by a small polyketide synthase gene cluster. *J. Biol. Chem.* **291**, 27403–27420 (2016).
66. Niehaus, E. M. *et al.* Sound of silence: The beauvericin cluster in *Fusarium fujikuroi* is controlled by cluster-specific and global regulators mediated by H3K27 modification. *Environ. Microbiol.* **18**, 4282–4302 (2016).
67. Gardiner, D. M., Jarvis, R. S. & Howlett, B. J. The ABC transporter gene in the sirodesmin biosynthetic gene cluster of *Leptosphaeria maculans* is not essential for sirodesmin production but facilitates self-protection. *Fungal Genet. Biol.* **42**, 257–263 (2005).
68. Miyazaki K, T. M. Creating random mutagenesis libraries using megaprimer PCR of whole plasmid. *Biotechniques* **33**, 1033–1038 (2002).
69. Kamitori, S., Iguchi, A., Ohtaki, A., Yamada, M. & Kita, K. X-ray structures of NADPH-dependent carbonyl reductase from *Sporobolomyces salmonicolor* provide insights into stereoselective reductions of carbonyl compounds. *J. Mol. Biol.* **352**, 551–558 (2005).
70. Jornvall, H. *et al.* Short-chain dehydrogenase/reductases (SDR). *Biochemistry* **34**, 6003–6013 (1995).
71. Filling, C. *et al.* Critical residues for structure and catalysis in short-chain dehydrogenases/reductases. *J. Biol. Chem.* **277**, 25677–25684 (2002).
72. Butler, Shane G., "Biochemical and biophysical characterization of a novel fumonisin detoxifying enzyme from *Aspergillus niger*" (2021). *Electronic Thesis and Dissertation Repository*. 7859. <https://ir.lib.uwo.ca/etd/7859at> references.
73. The Phyre2 web portal for protein modeling, prediction and analysis. Kelley LA *et al.* *Nature Protocols* **10**, 845–858 (2015).

Curriculum Vitae

Name: Michael Kovacevic

Post-secondary Education and Degrees: Western University
London, Ontario, Canada
2022-2025 J.D.

Western University
London, Ontario, Canada
2020-2022 M.Sc. (Biochemistry)

Western University
London, Ontario, Canada
2016-2020 B.MSc. (HSP Biochemistry)

Honours and Awards: Canada Graduate Scholarship-Master's (CGS-M) – NSERC
2020-2021

Ontario Graduate Scholarship (OGS) [Declined]
2020-2021

Western Graduate Research Scholarship (WGRS)
2020-2022

Related Work Experience Teaching Assistant – Biological Macromolecules (3381A)
Western University
Fall 2021

Research Assistant – Department of Chemistry & Chemical Biology
McMaster University (Biointerfaces Institute)
Summer 2019